

國立交通大學

光電工程研究所

碩士論文

氧離子佈植砷化鎵光導天線之 THz 輻射特性

THz radiation emission properties of oxygen-ion-implanted GaAs
photoconductive antennas

研究生：王韋文

指導教授：潘犀靈 教授

中華民國九十六年七月

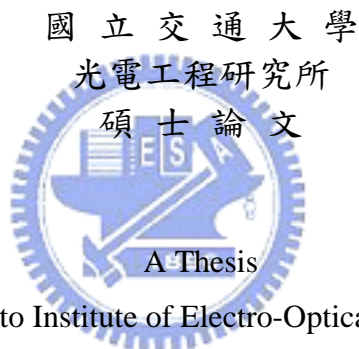
氧離子佈植砷化鎵光導天線之 THz 輻射特性
THz radiation emission properties of oxygen-ion-implanted GaAs
photoconductive antennas

研究生：王韋文

Student : Wei-Wen Wang

指導教授：潘犀靈 教授

Advisor : Prof. Ci-Ling Pan



Submitted to Institute of Electro-Optical Engineering
College of Electrical Engineering and Computer Science
National Chiao Tung University
In Partial Fulfillment of the Requirements
For the Degree of
Master of Engineering
In

Electro-Optical Engineering

July 2007

Hsinchu, Taiwan, Republic of China

中華民國九十六年七月

國立交通大學

博碩士論文全文電子檔著作權授權書

(提供授權人裝訂於紙本論文書名頁之次頁用)

本授權書所授權之學位論文，為本人於國立交通大學光電工程研究所，95年度第二學期取得碩士學位之論文。

論文題目：氧離子佈植砷化鎵光導天線之 THz 輻射特性

指導教授：潘犀靈

同意 不同意

本人茲將本著作，以非專屬、無償授權國立交通大學與台灣聯合大學系統圖書館：基於推動讀者間「資源共享、互惠合作」之理念，與回饋社會與學術研究之目的，國立交通大學及台灣聯合大學系統圖書館得不限地域、時間與次數，以紙本、光碟或數位化等各種方法收錄、重製與利用；於著作權法合理使用範圍內，讀者得進行線上檢索、閱覽、下載或列印。

論文全文上載網路公開之範圍及時間：

本校及台灣聯合大學系統區域網路	<input checked="" type="checkbox"/> 立即公開
校外網際網路	<input checked="" type="checkbox"/> 立即公開

授權人：王韋文

親筆簽名：_____

中華民國 年 月 日

國立交通大學

博碩士紙本論文著作權授權書

(提供授權人裝訂於全文電子檔授權書之次頁用)

本授權書所授權之學位論文，為本人於國立交通大學 光電工程 研究所，95 年度第 二 學期取得碩士學位之論文。

論文題目：氧離子佈植砷化鎵光導天線之 THz 輻射特性

指導教授：潘犀靈

■ 同意

本人茲將本著作，以非專屬、無償授權國立交通大學，基於推動讀者間「資源共享、互惠合作」之理念，與回饋社會與學術研究之目的，國立交通大學圖書館得以紙本收錄、重製與利用；於著作權法合理使用範圍內，讀者得進行閱覽或列印。



授權人：王韋文

親筆簽名：_____

中華民國 年 月 日

國家圖書館

博碩士論文電子檔案上網授權書

ID:GT009424526

本授權書所授權之學位論文，為本人於國立交通大學 電資 學院 光電工程 研究所，95 年度第 二 學期取得碩士學位之論文。

論文題目：氧離子佈植砷化鎵光導天線之 THz 輻射特性

指導教授：潘犀靈

茲同意將授權人擁有著作權之上列論文全文(含摘要)，非專屬、無償授權國家圖書館，不限地域、時間與次數，以微縮、光碟或其他各種數位化方式將上列論文重製，並得將數位化之上列論文及論文電子檔以上載網路方式，提供讀者基於個人非營利性質之線上檢索、閱覽、下載或列印。



※ 讀者基於非營利性質之線上檢索、閱覽、下載或列印上列論文，應依著作權法相關規定辦理。

授權人：王韋文

親筆簽名：_____

民國 年 月 日

1. 本授權書請以黑筆撰寫，並列印二份，其中一份影印裝訂於附錄三之二(博碩士紙本論文著作權授權書)之次頁；另一份於辦理離校時繳交給系所助理，由圖書館彙總寄交國家圖書館。

國立交通大學

論文口試委員會審定書

本校 光電工程研究所 碩士班 王韋文 君

所提論文：氧離子佈植砷化鎵光導天線之 THz 輻射特性

合於碩士資格水準、業經本委員會評審認可。

口試委員：

黃衍介

黃衍介 教授

林恭如

林恭如 教授

趙如蘋

趙如蘋 教授

陳瓊華

陳瓊華 助理教授

指導教授：

潘犀靈

潘犀靈 教授

所長：趙子飛 教授

系主任：董中乾 教授

中華民國九十年七月十六日

氧離子佈植砷化鎵光導天線之 THz 輻射特性

研究生：王韋文

指導教授：潘犀靈 教授

國立交通大學光電工程研究所

摘要

本論文討論在兩組多重氧離子佈植砷化鎵 (2.5×10^{13} ions/cm² (500 keV & 800 keV), 4×10^{13} ions/cm² (1200 keV) 和 6×10^{13} ions/cm² (500 keV & 800 keV), 1×10^{14} ions/cm² (1200 keV)) 薄膜材料，以此製作的偶極天線兆赫波的放射特性。

利用光脈衝寬約 100 飛秒、中心波長為 800 奈米的鎖模雷射激發氧離子佈植砷化鎵光導天線，與砷離子佈植砷化鎵光導天線 (~60KV/cm) 比較，前者可操作在較高的電場上 (~110KV/cm) 放射出高功率的兆赫波訊號，且具有較高的飽和光激發能量 (~45mW)。此外，改變光導天線的偶極長度也會影響到輻射波強度。該天線最大發射頻寬達 1.6THz，訊噪比最佳可達到 ~10000 以上。

最後，我們比較低溫成長砷化鎵與多重氧離子佈植砷化鎵偶極天線在輻射兆赫波上的差異性。在相同的光激發能量及電場下，我們發現後者可發射出較高的兆赫波訊號，強度 (~0.17μW) 約比低溫成長砷化鎵 (~0.09μW) 大上近一倍。雖然在頻寬上多重氧離子佈植天線和低溫成長砷化鎵天線還具有一段的差異，但由於多重佈植的方式在製程上比低溫成長來得更經濟，而且我們可以再去改變離子佈植濃度和退火溫度獲得更好的效果，因此在兆赫波的應用上還是具有相當的潛力。

THz radiation Emission Properties of Oxygen-ion-implanted GaAs Photoconductive Antennas

Student: Wei-Wen Wang

Advisor: Prof. Ci-Ling Pan

Institute of Electro-Optical Engineering
College of Electrical Engineering and Computer Science
National Chiao Tung University

Abstract

THz wave was generated from dipole antenna-type devices made by using Oxygen-ion implanted GaAs. We compared the emission properties of GaAs:O photoconductive (PC) antennas with different fabricated condition(2.5×10^{13} ions/cm² (500 keV & 800 keV), 4×10^{13} ions/cm² (1200 keV) and 6×10^{13} ions/cm² (500 keV & 800 keV), 1×10^{14} ions/cm² (1200 keV)) in the pulse mode. The absolute power of THz wave was also measured by a bolometer for comparison of the relative radiation power. High breakdown voltage threshold biasing (>110KV/cm) and large saturation optical pumping power (~45mW) in multi-GaAs:O based PC antennas are reported. THz radiation power is proportional to the effective antenna length and photocurrent.

We also compared the material multi-GaAs:O with low-temperature (LT) grown GaAs based on the same structure of PC antennas. The material multi-GaAs:O can generate higher THz power than LT-GaAs. It is almost 2 times higher for the GaAs:O (~0.17μW) than for the LT-GaAs (~0.09μW) under the same pump power (~35mW) and dc bias (~30V), respectively. Although the bandwidth of GaAs:O antennas is not broader than LT-GaAs, but it could be improved by optimizing the implant dosage and annealing temperature, and adopting other antenna structures for high frequency purpose. And the process of preparation for GaAs:O is easier than LT-GaAs. So it is promising as the substrate of the PC emitter antennas for THz radiation.

Acknowledgement

致謝

本論文得以順利的完成，首先要感謝指導老師潘犀靈教授的悉心教導，提供良好的研究資源和實驗環境，讓我可以順利完成實驗。在這兩年研究生活中，我真的很感謝黎宇泰學長在實驗上的協助及理論的指導，使我獲益良多。也很感謝香港中文大學陳錦泰教授實驗室的陳克堅學長幫忙製作的光導天線和提供許多寶貴的意見及經驗。此外，也謝謝實驗室的王怡超、陳晉璋學長們，及同學們：哲睿、彥毓、宜貞、君豪、昀甫因為有你們的陪伴，我的研究生生活才如此多采多姿，可以在枯燥的研究生活中帶來一些歡樂和喜悅，還有也謝謝學弟們：孟桓、介暉、育賢、松輝幫忙處理實驗室的事務及在實驗器材的協助，也因為有你們的鼓勵及幫助，我才能順利畢業。

最後，我要感謝我最親愛的家人：爸爸、媽媽和妹妹，在我求學過程中，一路上給予我最大的關懷與支持；也謝謝女友學雯，陪伴我這幾年一路走來，給我的支持及鼓勵，讓我無後顧之憂，順利完成碩士學位！謝謝。

于新竹 交大

2004/08/22

Table of Contents

Abstract	i.
Acknowledgements	iii.
Table of Contents	iv.
List of Figures	vi.
List of Tables	vii.
Chapter 1 Introduction	1.
1.1 Background.....	1.
1.2 Method of generating THz radiation	2.
1.2-1 Optical rectification	2.
1.2-2 Photoconductive switch	3.
1.3 Method of detecting THz radiation	5.
1.3-1 Liquid-helium cooled bolometer	5.
1.3-2 Photoconductive antenna	6.
1.3-3 Electro-Optical sampling	6.
1.4 Material of Photoconductor antenna	7.
1.4-1 Material of Low-temperature (LT) grown GaAs	7.
1.4-2 Material of ion-implanted GaAs	7.
1.5 Objective	8.
1.5-1 Motive.....	8.
1.5-2 Organization of this thesis.....	9.
Chapter 2 Basic Theory.	10.
2.1 The theory of generated THz radiation.....	10.
2.1-1 Current-surge model.....	11.
2.1-2 Drude-Lorentz model.....	16.
2.1-3 Photoconductor antenna with different structure....	18.
2.2 The properties of the material.....	19.
2.2-1 Choosing and analysis the material.....	19.
2.2-2 Dark current.....	20.
2.2-3 Photocurrent.....	21.

Chapter 3 Experiment Method and Setup	23.
3.1 Sample preparation	23.
3.1-1 Preparation of the PC antenna	24.
3.1-2 The setup of PC antenna.....	25.
3.2 Electric characteristics measurement.....	27.
3.2-1 Experiment setup.....	27.
3.2-2 The calibration of the Si bolometer	28.
3.2-3 Measurement result.....	30.
3.3 The time & frequency domain of THz pulse.....	30.
3.3-1 Martin-Puplett polarization interfered Spectrometer (FTIR)	30.
3.3-2 Terahertz Time-Domain Spectroscopy (THz-TDS)	33.
 Chapter 4 Result and Analysis	 35.
4.1 The result of Electric characteristics	35.
4.1-1 Current-voltage (I-V) curve	35.
4.1-2 THz power-voltage curve	36.
4.1-3 Analysis and Discussion.....	37.
4.2 THz radiation of GaAs:O antennas.....	40.
4.2-1 Measurement Result.....	40.
4.2-2 Different systems (FTIR & TDS)	46.
4.2-3 Analysis and Discussions.....	48.
4.3 Compare with LT-GaAs PC antenna	50.
4.3-1 Electric characteristics.....	51.
4.3-2 THz wave form & Spectrum	53.
 Chapter 5 Conclusion.....	 57.
5.1 Summary.....	57.
5.2 Future work.....	58.
 References.....	 60.

List of Figures

1.1-1	Electromagnetic spectrum.....	1.
1.2-1	Optical rectification	3.
1.2-2	Photoconductive switch.....	4.
2.1-1	Energy band structure of GaAs.....	10.
3.1-1	Schematic diagram of the PC antenna.....	23.
3.1-2	Schematic of focused the pump laser on the gap of dipole antennas.....	26.
3.2-1	Schematic of experiment setup for measure the electric characteristics of PC antenna.....	28.
3.3-1	Schematic of a Martin-Puplett-type Fourier Transform Infrared Spectrometer (FTIR) system.....	31.
3.3-2	The reflectivity of the electric field dependent with frequency under (a) parallel and (b) perpendicular component.....	33.
3.3-3	Terahertz Time-Domain Spectroscopy system.....	34.
4.1-1	I-V curve of oxygen ion-implant PC antennas with different dosage concentration and annealing temperature.....	36.
4.1-2	THz power-voltage curve of oxygen ion-implant PC antennas with different dosage concentration and annealing temperature.....	37.
4.1-3	Intensity of THz radiation measured as a function of the bias voltage for the GaAs:O PC antenna with different conditions. The pump power is fixed at 35mW.....	38.
4.1-4	Intensity of THz radiation measured as a function of the laser pump power for the GaAs:O PC antenna under the same antenna length. The bias is fixed at 15V.....	39.
4.2-1	The spectrum of different PC antennas (a) dipole 1 (b) dipole 3. The inset is the interfere waveform measured by FTIR system.....	41.
4.2-2	THz wave forms and spectrums of dipole 1 under (a) &(c) the different pump power and (b) & (d) the different bias.....	42.
4.2-3	The bias dependence of amplitude at the positive main peak in Dipole 3 under the same pump power.....	43.

4.2-4	The spectrum of different PC antennas (a) dipole 1 (b) dipole 3. The inset is waveform of electric pulse measured by TDS.....	45.
4.2-5	The comparison of spectrum with different measurement system in antenna of (a) Dipole 1 and (b) Dipole 3.....	47.
4.2-6	The THz wave form of the GaAs:O PC antenna under the different conditions and compared with LT-GaAs PC antenna.....	49.
4.2-7	The spectrum of the GaAs:O PC antenna under the different conditions.....	50.
4.3-1	The structure of PC antenna fabricated on GaAs:O and LT-GaAs material.....	51.
4.3-2	(a) Current-voltage curve measurements for GaAs:O and LT-GaAs PC antenna with pump power(~35mW) and without laser irradiation	52.
4.3-2	(b) THz power generated from GaAs:O and LT-GaAs PC antenna versus bias voltage under the same pump power (~35mW)	53.
4.3-3	THz wave form of GaAs:O PC antenna under (a) the different pump power and (b) the different bias.....	54.
4.3-4	The spectrum of dipole antenna with different substrate GaAs:O and LT-GaAs.....	55.

List of Tables

3.1	The antenna list.....	25.
-----	-----------------------	-----

Chapter 1 Introduction

1.1 Background

“Terahertz radiation” is the unit of electromagnetic radiation, which the frequency is near one trillion hertz (10^{12} Hz) as shown in Figure 1.1-1. THz radiation having a frequency of 1 THz has a wavelength of 0.3 millimeter (mm), or 300 micrometer (μ m). It is between microwave radiation and infrared radiation. Wireless transmissions and computer clock speed are at frequencies far below 1THz. In the past twenty years, terahertz radiation has already been researched in many domains. The THz radiation is not commonly used in computer and wireless technology, although it is possible that a microprocessor with a clock speed on 1 THz might be developed in the future. From some literatures, the THz radiation has been primarily developed on physicists and astronomers [01]. The imaging technology and spectroscopic technology are

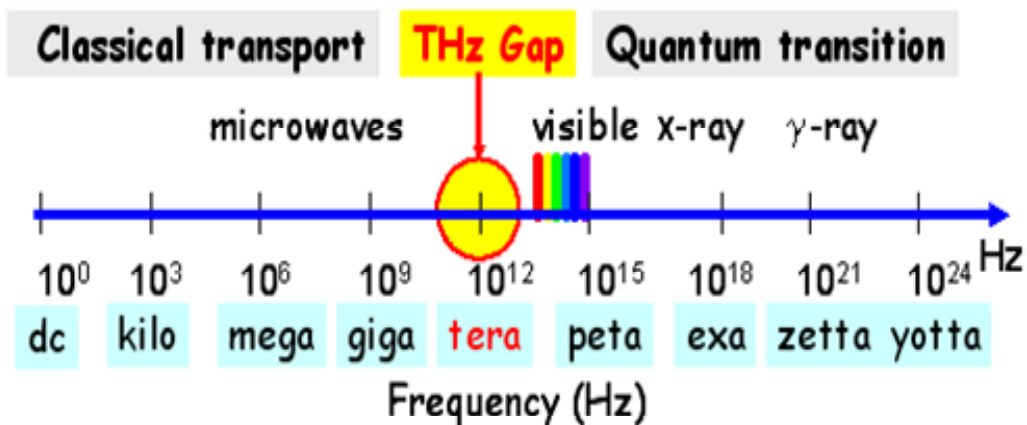


Figure 1.1-1 Electromagnetic spectrum.

(Refer to <http://www.wse.jhu.edu/~cmsd/THz/>)

studied in the Terahertz range [02]. Besides, it can be applied to measure not only medical but also materials inspection. There is great potential for its application in many other scientific fields as well. In order to generate THz radiation, the femto-second pulse laser is the usual optical source, such as Ti-sapphire laser, which is expensive and large size. This kind of laser is not usually available in laboratories. Besides, there is a different source to generate THz radiation. Using semiconductor laser diode can generate the continuous wave THz radiation.

1.2 Method of generating THz radiation

Due to the recent development of pico-second and femto-second laser system, there are various ways to generate the ultrashort pulsed millimeter and submillimeter radiation [03], such as optical rectification and resonant THz radiation in photoconductor generated by a pulse laser or a pair of continuous wave laser.

1.2-1 Optical rectification

Optical rectification is the nonlinear effect of the second order characteristic. In the electro-optic medium, the low frequency electric field is produced under intense optical illumination. Optical rectification in a non-absorbing medium is a process in which a laser pulse creates a time-dependent polarization that radiates an electric field which can be written as $\vec{E}(t) \propto \frac{\partial^2 \vec{P}}{\partial t^2}$ in the far field, where the

polarization P follows the pulse intensity envelope. It is called rectification because the rapid oscillations of the electric field of the pulse laser are “rectified” and only the envelope of the oscillations remains. There is the schematic setup in Figure 1.2-1. Since the medium is nonabsorbing, the polarization instantaneously follows the pulse envelope implying that there is practically no limit on the speed at which the polarization can be switched on and off. The incident of polarization wave radiates a transient electric field which consists of one or one-and-a-half oscillation and therefore has a broadband THz frequency bandwidth. Bandwidth as large as 30 THz has been obtained using this generation mechanism.

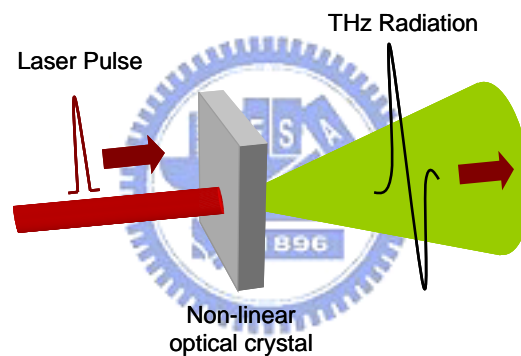


Figure 1.2-1 Optical rectification

1.2-2 Photoconductive switch

This mechanism of generated THz radiation from the biased photoconductive switch is generally based on the theory, which is called “current surge model” [04]. We will discuss the basic theory of this model in detail in next chapter. According to this model, as the energy of the input laser is higher than the energy of bandgap of photoconductor, then electron-hole pairs are excited and the

mechanism of generated THz radiation can occur.

In briefly, the electromagnetic field of THz radiation is generated from a transient current which is generated on the surface of the photoconductor. The pulse laser generates carriers instantaneously. We add a bias to accelerate the carriers. Then, the resultant transient current, or be called current surge, produces an electric field on the surface of the photoconductor. This surface electric field is regarded as the source of the THz radiation. Figure 1.2-2 shows the setup for this method.

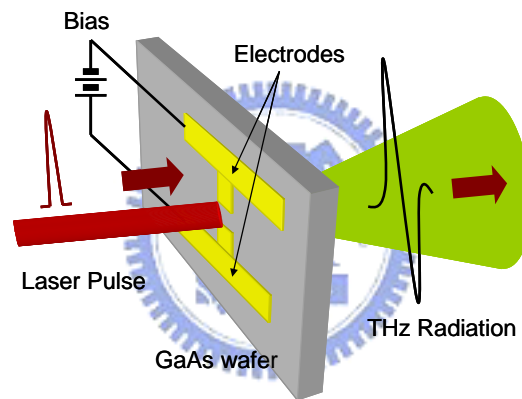


Figure 1.2-2 Photoconductive switch

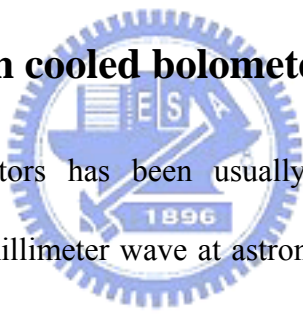
We put two electrodes on the top of substrate which can use different materials, such as GaAs, low temperature grown GaAs (LT-GaAs). This photoconductor behaved as an isolation without illuminate optical source. When we give the voltage across two electrodes and illuminate the region between two electrodes, the substrate becomes conducting. Under the influence of the applied electric field, current starts to flow. A time dependent current can also radiate transient electric field with a higher efficiency than optical rectification. The

frequency contents of this transient are determined by the transient behavior of the current and have 3dB bandwidth of 1 THz typically and roughly.

1.3 Method of detecting THz radiation

In the traditional method, THz radiation is generated by heat source and detected by liquid-helium cooled bolometer. In addition, there are different ways which are developed in recent years to detect THz radiation, such as photoconductive antenna and electro-optic sampling (EO sampling).

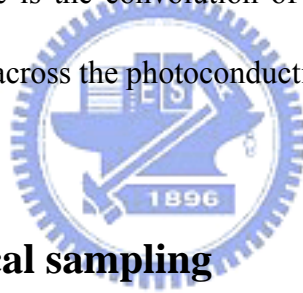
1.3-1 Liquid-helium cooled bolometer



This kind of detectors has been usually used for far-infrared (FIR), submillimeter wave and millimeter wave at astronomy in the past 40years. A hot electron bolometer is a device. When it absorbs the incident radiation, the resistance would responds to the change of electron's temperature. A traditional bolometer consists of a heat-sensitive detection element mounted inside a heat sink and physically supported by a thermally conductive physical supporter. The most common systems are helium-cooled Si, Ge and InSb bolometer. It can measure the radiation power lower to nanowatt grade, but it losses the information of phase and frequency. Because of it, using bolometer to detect the power of THz radiation usually accompanies Martin-Puplett interferometer [05]. By using this system, we can obtain the interferogram of THz radiation [06]. We will detail this system in next chapter.

1.3-2 Photoconductive antenna

The photoconductive detector is using photoconductive antenna as the detector [07]. When the incident THz radiation illuminates the photoconductive antenna, it induces transient current and then accelerate electron by probe beam. In this kind of detectors, two factors determine the spectrum bandwidth. One of them is the photocurrent response (i.e. carrier lifetime) and the other one is the frequency dependence of the antenna structure [08-09]. In general, the low frequency cutoff of the detectors results from the collection efficiency of the dipole, while the upper frequency limit is determined by the photocarrier response. The photocurrent response is the convolution of the transient photoconductivity and the THz electric field across the photoconductive antenna.



1.3-3 Electro-Optical sampling

The detector of Electro-Optical (EO) sampling has broad bandwidth spectrum and is easy to implement. Recently, technique of EO sampling has become an alternative to PC detection [10]. The Zinc-Blende crystal was used to measure THz radiation based on the Pockels effect [10]. When we vary the temporal delay between pump and probe beam, the synchronous probe beam will probe the transient change of refractive index result from THz radiation changing the refractive index. There is a trade-off in this method, so thickness of the crystal plays an important role. Thick crystal will introduce longer interaction length but reduce the frequency response.

1.4 Material of Photoconductor antenna

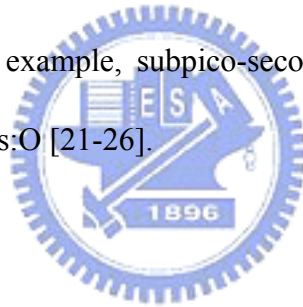
1.4-1 Material of Low-temperature (LT) grown GaAs

Low-temperature (LT) grown GaAs is widely used as the photoconductive substrate of PC antennas for generation and detection of THz radiation because of the high resistivity ($10^7 \Omega cm$) [11] and good mobility ($100-300 cm^2 / Vs$) [12-13], in addition to short carrier lifetime ($< 1 ps$) [14-15]. These excellent characteristics are however difficult to reproduce from sample because the quality of the material depends critically on both the growth temperature and the post growth thermal annealing conditions. An alternative material was reported to be promising as the substrate material of PC antennas, which is the arsenic ion-implanted GaAs [16]. These materials exhibit good structural and electrical properties and show ultrafast optoelectronic response. It is again possible to improve the carrier mobility of these ion-bombarded materials using postimplantation thermal annealing process. Good control over the overall fabrication process allows studies of the influence of parameters such as the ion-implantation dose, the ion energy, and the thermal annealing conditions on the PC antenna characteristics.

1.4-2 Material of ion-implanted GaAs

The arsenic (As) ion implanted GaAs PC antennas have shown to be better THz emitters than those made on semi-insulating (Si) GaAs substrates [17-20]. It

has demonstrated that the terahertz emission property of arsenic ion-implanted GaAs has almost the same characteristics with Low-temperature (LT) grown GaAs. Such enhancement results from ultrafast carrier recombination associated with the presence of the implantation-induced defects. On the other hand, several groups have shown good characteristics of THz emitters with the use of PC antennas made on GaAs substrates grown by the Czochralski method when these devices are photoexcited near the anode. Although defects seem to play a crucial role in the characteristics of THz PC antenna emitters, there are very few studies that investigate the role of defects on these characteristics. Ion-implantation using other types of ions has already been used successfully to reduce the carrier lifetime in Si GaAs. For example, subpico-second lifetime can be obtained in GaAs:H GaAs:N and GaAs:O [21-26].



1.5 Objective

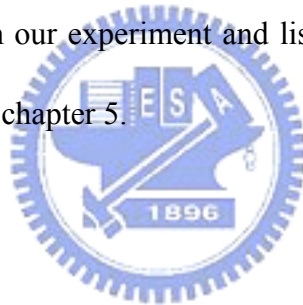
1.5-1 Motive

In this thesis, we used the pulse laser to measure the characteristics of the terahertz emitter fabricated on the substrates of Oxygen ion-implanted GaAs which have the different multi-implants dosage concentrations and annealing temperatures. We compared the emission properties of GaAs:O PC antennas under the different bias and pump power. And we measure the spectrums of our samples to compare with other material.

1.5-2 Organization of this thesis

There are mainly five chapters in the thesis, consisting of introduction (Ch.1), basic theory (Ch.2), experiment setup and method (Ch.3) result and analysis (Ch.4) and conclusion (Ch.5).

In chapter 1, we introduce the background of THz radiation and describe the motivation of the researching work. The basic theories about THz radiation generated from dipole antenna are mentioned in chapter 2. The experiment setup and measuring procedure are shown in chapter 3. And in chapter 4, the results of the researching and analysis are discussed. Finally, we will give a summary about the researching work from our experiment and list some future works which can be studied continuously in chapter 5.



Chapter 2 Basic Theory

In this chapter, the most important part is to introduce the basic theory of generated and detected THz radiation using photoconductor antenna. And then, we introduce the properties of material which will be the substrates of PC antennas.

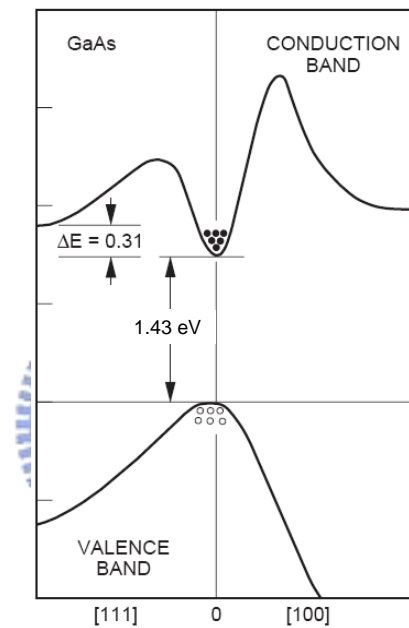


Figure 2.1-1 Energy band structure of GaAs

2.1 The theory of generated THz radiation

As we illuminated the photoconductor antenna and the optical power is greater than the energy gap of semiconductor which is the substrate of the photoconductor antenna. The Energy band structure of GaAs has is shown in Figural 2.1-1. Then, this semiconductor will absorb the energy of incident wave and generate free electron-hole pair at the same time. We give bias to the electrode

of the photoconductor antenna; it can accelerate the carrier which is generated by incident wave. The brief surface current will be generated. This process can find expression in the Current-surge model.

2.1-1 Current-surge model

The first step, there are some time-average parameters which we need to define the THz radiation [22].

Charge density $\Rightarrow \rho(x,y,z,t)$

Current density $\Rightarrow \vec{J}(x,y,z,t)$

Electric field intensity $\Rightarrow \vec{E}(x,y,z,t)$

Magnetic flux density $\Rightarrow \vec{B}(x,y,z,t)$

Then, it is necessary to construct Maxwell's equation for Current-surge model.

From Maxwell's equation [28]:

$$\nabla \times \vec{E} = -\frac{\partial \vec{B}}{\partial t} \quad (\text{Faraday's Law}) \quad (2.1-1)$$

$$\nabla \cdot \vec{E} = \frac{\rho}{\varepsilon} \quad (\text{Gauss Law}) \quad (2.1-2)$$

$$\nabla \times \vec{H} = \vec{J} + \frac{\partial \vec{D}}{\partial t} \quad (\text{Ampere's Law}) \quad (2.1-3)$$

$$\nabla \cdot \vec{B} = 0 \quad (2.1-4)$$

And we know

$$\vec{B} = \nabla \times \vec{A} \quad (2.1-5)$$

From Equation (2.1-1) and (2.1-5), we get:

$$\nabla \times \vec{E} = -\frac{\partial \vec{B}}{\partial t} = -\frac{\partial}{\partial t} (\nabla \times \vec{A}) = \nabla \times \left(-\frac{\partial \vec{A}}{\partial t} \right) \Rightarrow \nabla \times \left(\vec{E} + \frac{\partial \vec{A}}{\partial t} \right) = 0 \quad (2.1-6)$$

Then, we set a non-vector value V and employ that $\nabla \times \nabla V = 0$ to substitute the Equation (2.1-6).

$$-\nabla V = \vec{E} + \frac{\partial \vec{A}}{\partial t} \Rightarrow \vec{E} = -\nabla V - \frac{\partial \vec{A}}{\partial t} \quad (2.1-7)$$

From Equation (2.1-3) , (2.1-5) and $\vec{H} = \frac{\vec{B}}{\mu}$, $\vec{D} = \epsilon \vec{E}$, we obtain

$$\frac{\nabla \times \vec{B}}{\mu} = \vec{J} + \epsilon \frac{\partial \vec{E}}{\partial t} \Rightarrow \nabla \times (\nabla \times \vec{A}) = \mu \left(\vec{J} + \epsilon \frac{\partial \vec{E}}{\partial t} \right) \quad (2.1-8)$$

Substitute Equation (2.1-7) into Equation (2.1-8)

$$\begin{aligned} \nabla \times (\nabla \times \vec{A}) &= \mu \left[\vec{J} + \epsilon \frac{\partial}{\partial t} \left(-\nabla V - \frac{\partial \vec{A}}{\partial t} \right) \right] \\ \nabla (\nabla \cdot \vec{A}) - \nabla^2 \vec{A} &= \mu \vec{J} - \mu \epsilon \nabla \frac{\partial V}{\partial t} - \mu \epsilon \frac{\partial^2 \vec{A}}{\partial t^2} \\ \Rightarrow \nabla^2 \vec{A} - \mu \epsilon \frac{\partial^2 \vec{A}}{\partial t^2} &= -\mu \vec{J} + \nabla \left(\nabla \cdot \vec{A} + \mu \epsilon \frac{\partial V}{\partial t} \right) \end{aligned} \quad (2.1-9)$$

From Equation (2.1-2) and $\vec{D} = \epsilon \vec{E}$

$$\begin{aligned} \nabla \cdot (\epsilon \vec{E}) &= -\nabla \cdot \left[\epsilon \left(\nabla V + \frac{\partial \vec{A}}{\partial t} \right) \right] = \rho \\ \Rightarrow \nabla^2 V + \frac{\partial}{\partial t} (\nabla \cdot \vec{A}) &= -\frac{\rho}{\epsilon} \end{aligned} \quad (2.1-10)$$

Because of Lorentz gauge $\nabla \cdot \vec{A} + \epsilon \mu \frac{\partial V}{\partial t} = 0$, Equation (2.1-9) becomes as

$$\nabla^2 \vec{A} - \mu \epsilon \frac{\partial^2 \vec{A}}{\partial t^2} = -\mu \vec{J} \quad (2.1-11)$$

And, Equation (2.1-10) can be written as

$$\nabla^2 V - \mu \epsilon \frac{\partial^2 V}{\partial t^2} = -\frac{\rho}{\epsilon} \quad (2.1-12)$$

Equation (2.1-11) and (2.1-12) are the two inhomogeneous wave equations written in terms of \vec{A} and V . The two wave equations are used to determine a functional

and time dependent of the radiated electric field in the far field.

From Equation (2.1-3), the continuity equation of the free carriers is obtained.

$$\nabla \cdot (\nabla \times \vec{H}) = \nabla \cdot \left(\vec{J} + \frac{\partial \vec{D}}{\partial t} \right) = \nabla \cdot \vec{J} + \frac{\partial \rho}{\partial t} = 0 \quad (2.1-13)$$

In the fact, the current density of the photoconductor antenna which adds the bias is the transverse current, parallel the surface of the photoconductor antenna and perpendicular the direction of propagation. So that

$$\nabla \cdot \vec{J} = 0 \quad (2.1-14)$$

From Equation (2.1-13) and (2.1-14), we can deduce that the charge density does not vary with time and not contribute the time dependent radiated electric field. As the result, Equation (2.1-7) becomes

$$\vec{E}(\vec{r}, t) = -\frac{\partial}{\partial t} \vec{A}(t) \quad (2.1-15)$$

The solution of the vector potential \vec{A} in Equation (2.1-11) leads into the Equation (2.1-15) to express the time dependent radiated electric field $\vec{E}_{\text{rad}}(\vec{r}, t)$ at the displacement \vec{r} from the center of the photoconductor antenna.

$$\vec{E}_{\text{rad}}(\vec{r}, t) = -\frac{1}{4\pi\epsilon_0 c^2} \frac{\partial}{\partial t} \int \frac{\vec{J}_s \left(\vec{r}', t - \frac{|\vec{r} - \vec{r}'|}{c} \right)}{|\vec{r} - \vec{r}'|} da' \quad (2.1-16)$$

where ϵ_0 is the permittivity of free space, c is the speed of light in vacuum, \vec{J}_s is the surface current of the photoconductor antenna in the retarded time, and da' is the increment of surface area at the displacement \vec{r}' from the center of the photoconductor antenna. The integration is covered with whole the optically

illuminated area of the photoconductor antenna. In the far field,

$$|\vec{r}-\vec{r}'| = r \left(1 - \frac{\hat{n} \cdot \vec{r}'}{r} \right) \approx r \quad (2.1-17)$$

The gap between the electrodes of the photoconductor antenna is assumed to be uniformly illuminated by the optical source. Therefore, the surface current \vec{J}_s can be set as a constant in space. Then, the radiated electric field in Equation (2.1-16) can be written as

$$\vec{E}_{\text{rad}}(\vec{r}, t) = -\frac{1}{4\pi\epsilon_0 c^2} \frac{A}{r} \frac{\partial}{\partial t} \vec{J}_s \left(t - \frac{r}{c} \right) \quad (2.1-18)$$

where A is the illuminated area of the photoconductor antenna and $r = \sqrt{x^2 + y^2 + z^2}$. We considered that the THz radiation is generated on Z axis (i.e. $x = y = 0$), and let $t \rightarrow t - \left(\frac{z}{c} \right)$. Thus, The Equation (2.1-18) can be written as

$$\vec{E}_{\text{rad}}(\vec{r}, t) = -\frac{1}{4\pi\epsilon_0 c^2} \frac{A}{z} \frac{\partial}{\partial t} \vec{J}_s(t) \quad (2.1-19)$$

Beside, we can know the equation (2.1-20) from surface current [29].

$$\vec{J}_s(t) = \frac{\sigma_s(t) \vec{E}_b}{\frac{\sigma_s(t) \eta_0}{1+n} + 1} \quad (2.1-20)$$

where n is the refractive index of photoconductor antenna under the wavelength of μm . η_0 is the impedance in free space, and $\sigma_s(t)$ is the surface conductivity which is shown in the equation (2.1-21).

$$\sigma_s(t) \equiv \frac{e(1-R)}{\hbar\omega} \int_{-\infty}^t dt' m(t, t') I_{\text{opt}}(t') \exp\left[-\frac{-(t-t')}{\tau_{\text{car}}}\right] \quad (2.1-21)$$

where e is the electric charge, R is the reflectivity of photoconductor antenna, $\hbar\omega$ is the photon energy, $m(t, t')$ is the time-dependent carrier mobility at time t from created carrier at time t' , I_{opt} is the time-dependent of optical intensity, and τ_{car} is the carrier lifetime of excited carriers. For the present derivation, we

assume that carrier mobility is a constant.

$$m(t, t') = m \quad (2.1-22)$$

And assume that the carrier lifetime is long enough, $\tau_{car} \rightarrow \infty$. A Gaussian intensity profile of the optical beam is assumed:

$$I_{opt}(t') = I_0 \exp\left(\frac{-t'^2}{\tau^2}\right) \quad (2.1-23)$$

From these assumptions, the surface conductivity becomes

$$\sigma_s(t) \equiv \frac{e(1-R)}{\hbar\omega} I_0 \int_{-\infty}^t dt' m \exp\left(\frac{-t'^2}{\tau^2}\right) \quad (2.1-24)$$

From the equation (2.1-20) and (2.1-24) lead to the equation (2.1-19).

$$\vec{E}_{rad}(\vec{r}, t) = \frac{1}{4\pi\epsilon_0 c^2} \frac{A e(1-R)}{z} \frac{I_0 m \exp\left(\frac{-t^2}{\tau^2}\right)}{\hbar\omega} \times \left[1 + \frac{\eta_0 e(1-R) I_0 m}{(n+1)\hbar\omega} \int_{-\infty}^{t/\tau} \tau \exp(-x^2) dx \right]^{-2} \quad (2.1-25)$$

Comparing with the result from experiment, it is necessary to rewrite the equation (2.1-25) in term of the experimental parameters E_b which is the bias electric field applied across the photoconductor, and F_{opt} which is the incident optical intensity.

$$F_{opt} = \int_{-\infty}^{\infty} I_0 \exp\left(\frac{-t^2}{\tau^2}\right) dt = \sqrt{\pi} I_0 \tau \equiv \frac{E_{opt}}{A} \quad (2.1-26)$$

where E_{opt} is the average optical energy and A is the area of the incident optical beam. Then we define the parameter B and D to simplify the equation.

$$B = \frac{A e(1-R) m}{4\pi\epsilon_0 c^2 z \hbar\omega \sqrt{\pi}} \quad (2.1-27)$$

$$D = \frac{\eta_0 e(1-R) m}{(n+1)\hbar\omega \sqrt{\pi}} \quad (2.1-28)$$

And then, the electric field in the far field can be written as

$$E_{rad}(t) = -B E_b \frac{F_{opt}}{\tau} \exp\left(\frac{-t^2}{\tau^2}\right) \times \left[1 + D F_{opt} \int_{-\infty}^{t/\tau} \exp(-x^2) dx \right]^{-2} \quad (2.1-29)$$

Beside of current surge model, we can also discuss on the point of the carrier

dynamics in semiconductor to analyze the THz generation by Drude-Lorentz model when we need to discuss the factor of material in photoconductive antenna [30-31].

2.1-2 Drude-Lorentz model

For the calculation of carrier transport and THz radiation in a biased semiconductor, the one-dimensional Drude-Lorentz model is used. When a biased semiconductor is pumped by a laser pulse with photon energies greater than the band gap of the semiconductor, electrons and holes will be created in the conduction band and valence band, respectively. The carrier pumped by ultrashort laser pulse is trapped in the mid-gap states with the time constant of the carrier trapping time. The time-dependence of carrier density is given by the following equation.

$$\frac{dn(t)}{dt} = -\frac{n(t)}{\tau_c} + G(t) \quad (2.1-30)$$

where $n(t)$ is the density of the carrier, $G(t)$ is the generation rate of the carrier by the laser pulse, and τ_c is the carrier trapping time. The generated carriers will be accelerated by the bias electric field. The acceleration of electrons (holes) in the electric field is given by

$$\frac{d\nu_{e,h}(t)}{dt} = -\frac{\nu_{e,h}(t)}{\tau_s} + \frac{q_{e,h}}{m_{e,h}} E \quad (2.1-31)$$

where $\nu_{e,h}(t)$ is the average velocity of the carrier, $q_{e,h}$ is the charge of an electron (a hole), $m_{e,h}$ is the effective mass of the electron (hole), $\tau_{e,h}$ is the momentum relaxation time, and E is the local electric field. The subscript e and h

represent electron and hole, respectively. The local electric field E is smaller than the applied bias electric field E_b , due to the screening effects of the space charges,

$$E = E_b - \frac{P}{\alpha\varepsilon} \quad (2.1-32)$$

where P is the polarization induced by the spatial separation of the electron and hole, ε is the dielectric constant of the substrate and α is the geometrical factor of the photoconductive material. The geometrical factor α is equal to three for an isotropic dielectric material. It is noted that both, the free and trapped carriers contribute to the screening of the electric field. The time dependence of polarization P can be written as

$$\frac{dP}{dt} = -\frac{P}{\tau_r} + J \quad (2.1-33)$$

where τ_r is the recombination time between an electron and hole. In the equation (2.1-33), J is the density of the current contributed by an electron and hole,

$$J = en\nu_h - en\nu_e \quad (2.1-34)$$

where e is the charge of a proton. The change of electric currents leads to electromagnetic radiation according to Maxwell's equations. In a simple Hertzian dipole theory, the far-field of the radiation E_{THz} is given by

$$E_{\text{THz}} \propto \frac{\partial J}{\partial t} \quad (2.1-35)$$

To simplify the following calculations, we introduce a relative speed ν between an electron and hole,

$$\nu = \nu_h - \nu_e \quad (2.1-36)$$

Then the electric field of THz radiation can be expressed as

$$E_{\text{THz}} \propto e\nu \frac{\partial n}{\partial t} + en \frac{\partial \nu}{\partial t} \quad (2.1-37)$$

The first term on the right hand side of the equation (2.1-37) represents the electromagnetic radiation due to the carrier density change, and the second term represents the electromagnetic radiation which is proportional the acceleration of the carrier under the electric field.

2.1-3 Photoconductor antenna with different structure

In our experiment, we used the different structure of PC dipole antennas to radiate THz wave. According to the literature [32] and equation (2.1-35), the radiation E_{THz} can be written as:

$$E_{\text{THz}}(t) \propto l_e \frac{\partial J(t)}{\partial t} \quad (2.1-38)$$

where l_e is the effective length of the dipole. From Equation (2.1-38), the amplitude of THz radiation is influenced by the effect length and time-dependence photocurrent. The effect of current will be discussed on next section. The effect length relate to the structure of PC antenna. The larger effective length of the dipole can get the larger amplitude of THz radiation.

2.2 The properties of the material

2.2-1 Choosing and analysis the material

In order to generate high power and broadband THz radiation, two properties are necessary for the material. One of properties is short carrier lifetime, and another is high carrier mobility. Because of them, PC antenna could be generated the shorter pulse. However, it can't give consideration to two conditions. When we create the more recombination centers in semiconductor, it can trap carriers by using recombination centers to decrease the carrier lifetime. To create the more recombination centers, we implant the more defect in substrate and from deep level recombination. However, implanting the more defect, the structure of the crystal will be destroyed and decrease the carrier mobility.

$$\tau_c = \frac{1}{N_t \sigma_c \langle \nu_{th} \rangle} \quad (2.2-1)$$

$$\mu \approx \frac{1.4 \times 10^{22}}{N_t} \frac{m_0 \varepsilon_0}{m^* \varepsilon} \quad (2.2-2)$$

m_0 : the original mass of carrier

m^* : the effective mass of carrier

ε_0 : quasi-static dielectric constant

ε_r : relative dielectric constant

$$\varepsilon = \varepsilon_0 \varepsilon_r$$

N_t : defect density

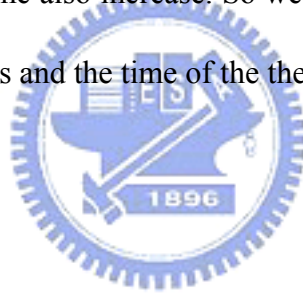
μ : carrier mobility

τ_c : carrier lifetime

σ_c : capture cross section

$\langle v_{th} \rangle$: mean thermal velocity

According to the Equation (2.1-1) and (2.1-2), we can know that the shorter carrier lifetime the less carrier mobility. It means that we decrease the carrier lifetime by implanting defects and the carrier mobility also decrease at the same time. Because of it, we use the way which is thermal annealing process to solve this problem. The thermal annealing processes can rearrangement the crystal of material which implanted defects. It can increase some of the carrier mobility. However, the carrier lifetime also increase. So we need to do the balance between the concentration of defects and the time of the thermal annealing process.



2.2-2 Dark current

In theory, there is no current generated from PC antenna which applies voltage, when it does not illuminate leaser beam yet. However, we can measure a few current in PC antenna, which we call dark current. In general, the theory of current transport of the metal-semiconductor junction potential barrier is mainly drift, diffusion, and tunneling effect. It's contribution is in relation to intrinsic potential barrier $q\Phi_B$, built-in electric potential V_{bi} and applied voltage. In order to avoid generating rectification effect and junction resistance on the metal-semiconductor junction, it is usually using the process of implant high concentration of defect in semiconductor to increase built-in electric potential and

decrease the width of depletion region. So the carrier can easily through the junction potential as applying voltage. It is the process of Ohm contact.

2.2-3 Photocurrent

Comparing with dark current, Photocurrent means that it generated from PC antenna which applies voltage, when it illuminates leaser beam. We use the ultra-pulse laser to incident into the gap on the photoconductor antenna, and generate the transient photocurrent to radiate THz electromagnetic pulse. The value of photocurrent is in relation to the bias value and the power of the leaser beam. It can express as:

$$I = \frac{V_{bias}}{R_0 + R(t)} = \frac{V_{gap}}{R(t)} \approx \frac{V_{bias}}{R(t)} \quad (2.2-3)$$

R_0 is time-independence value of resistance. It can divide into two parts, one is contact resistance and the other is load resistance. $R(t)$ is time-dependence value of resistance which photoconductor illuminates leaser beam. We set that there is an incident beam on the photoconductor and using the photon energy generate the electron-hole pair. And them, the photoconductor parameter σ can be expressed as:

$$\sigma = q(\mu_n + \mu_p)\Delta n \quad (2.2-4)$$

where q is the charge of electron, μ_n and μ_p are the mobility of electron and hole. Δn is the density of carrier. If the average power of incident optical pulse is P_{avg} and photon energy is $h\nu$. The carrier generation rate G per unit volume can express as:

$$G = \eta \frac{P_{\text{avg}}}{h\nu\tau_{\text{pw}} QV_0} \quad (2.2-5)$$

where η is the quantum effect, τ_{pw} is the bandwidth of leaser pulse, Q is the repetition rate of leaser pulse and V_0 is the total volume of activity region.

Under the steady state, the carrier generation rate G is:

$$G = \frac{\Delta n}{\tau_{\text{pw}}} \quad (2.2-6)$$

$$\therefore \sigma = q(\mu_n + \mu_p)\Delta n = q(\mu_n + \mu_p)G\tau_{\text{pw}} \quad (2.2-7)$$

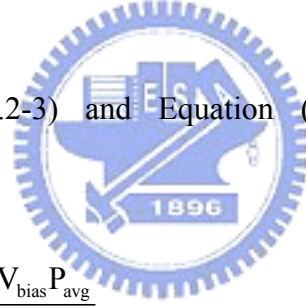
From Equation (2.2-7), we can get the optical resistance R_p .

$$R_p = \frac{L}{\sigma A} = \frac{h\nu QL^2}{q\eta(\mu_n + \mu_p)P_{\text{avg}}} \quad (2.2-8)$$

where A is the cross-section area of activity region and L is the length of activity region.

From Equation (2.2-3) and Equation (2.2-8), we can express the photocurrent as:

$$I = \frac{V_{\text{bias}}}{R_p} = \frac{q\eta(\mu_n + \mu_p)V_{\text{bias}}P_{\text{avg}}}{h\nu QL^2} \quad (2.2-9)$$



Chapter 3 Experiment Method and Setup

In this chapter, we introduce the samples which are fabricated as our substrates of PC antenna. And then, we introduce the experiment methods and setups for measure some emission properties of THz radiation.

3.1 Sample preparation

In our experiment, we employed the dipole antenna as our antenna structure. This kind of structure has been demonstrated to obtain a large signal and high bandwidth [31]. The detail structure of the PC antenna has been shown in Figure 3.1-1. And, Knon et al. proved that the spectral response of the PC antenna for broadband detection is mainly determined by the temporal behavior of the number of photo-excited carriers [15].

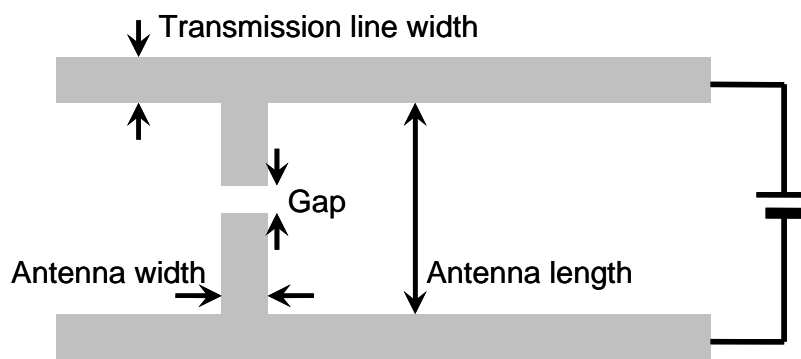
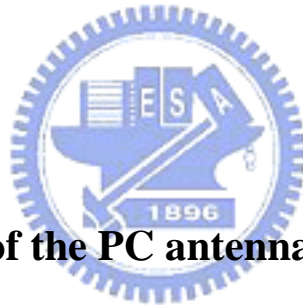


Figure 3.1-1 Schematic diagram of the PC antenna

Recently, Salem et al. [25] introduce oxygen ion as the dose to optimize the characteristics of GaAs substrate and generated THz waves from it. Normally, oxygen ion is looked as dust (not good thing) for electrical devices fabrication during the process, as its existence should make the contacts be not Ohmic-contact. But, in this case (material for THz wave generation), it looks its advantages are more than its disadvantages. As the electrical level formed by oxygen ion in GaAs is close to Fermi-level, it makes the oxygen ion implanted GaAs close to electrically neutral and has comparative high resistance. This kind of material also can have high breakdown voltage and considerable short carrier lifetime by implanted under certain high dosage and annealed under suitable annealing temperature.



3.1-1 Preparation of the PC antenna

We used multi-implanted GaAs:O as the substrate and then fabricated dipole antenna on it. From some papers [22-23, 25], the GaAs:O is further studied. They show that this kind of material really has some advantages for THz waves generation, and can generate higher power and higher frequency if we can optimize the implant dosage, annealing temperature and introduce some antenna design for high frequency purpose.

We optimize the dosage and the implanted energy to match the requirements. Considering the cost of time for RBS facility, we prepare two kinds of sample which have different implanted dosage concentration and annealing temperature

as the dipole antenna structure. In implanting process, one of samples multi-implants dosage concentrations is 2.5×10^{13} ions/cm² (500Kev & 800Kev) and 4×10^{13} ions/cm² (1200kev) and the other sample multi-implants the higher dosage concentrations is 6×10^{13} ions/cm² (500Kev & 800Kev) and 1×10^{14} ions/cm² (1200kev). After implantation process, we do the thermal annealing by RTA (Rapid Temperature Annealing) under N₂ gas environment and use a GaAs cap to prevent As ion desorption. In our experiment, one of the parameter of RTA is 550°C for 60s and the other is 500°C for 60s. (For reference, under 500°C for 60s annealing, the resistance of this GaAs:O substrate is close to 1.26×10^7 (Ω/sq)) And we prepared different structure of antenna length for measure THz radiation. The detail sample list is shown in the Table 3.1.

Table 3.1 The antennas list

Substrate	Dosage Condition	Annealing Temperature	Antenna length and width (L/W)	Photo-conductive Gap(G)	Transmission Line width (D)	Device Type
GaAs:O	500KeV/6e13	300°C/5s	200/25 μm	20 μm	25 μm	Dipole 1
	800KeV/6e13	550°C/60s	100/25 μm	20 μm	25 μm	Dipole 2
	1200KeV/1e14					
	500KeV/2.5e13	300°C/5s	100/25 μm	20 μm	25 μm	Dipole 3
	800KeV/2.5e13	500°C/60s	50/25 μm	20 μm	25 μm	Dipole 4
	1200KeV/4e13					

3.1-2 The setup of PC antenna

After prepare the PC antenna, we put the PC antenna on the mount which we

design. The pump laser could be focused on the dipole by the objective lens. And then, we use the silicon lens to decrease the angle of the THz radiation outgoing the substrate. The type of our silicon lens is hyper-hemispherical lens, the radius is 6.75mm and the total thickness is 8.35mm. There are two steps to make sure the pump laser is focused on the gap of the dipole antenna. The first step, we use a thin glass and put it before the objective lens. Then, we can see the image on the screen which is reflected from the dipole antenna and check the location of focused laser beam on the sample. The detail experiment method is shown in the Figure 3.1-2. After check the correct location, the next step is contact the multi-meter to the dipole antenna for measure the resistance, and optimizes the objective lens and incident pump beam to search the minimum value of resistance as possible as we can.

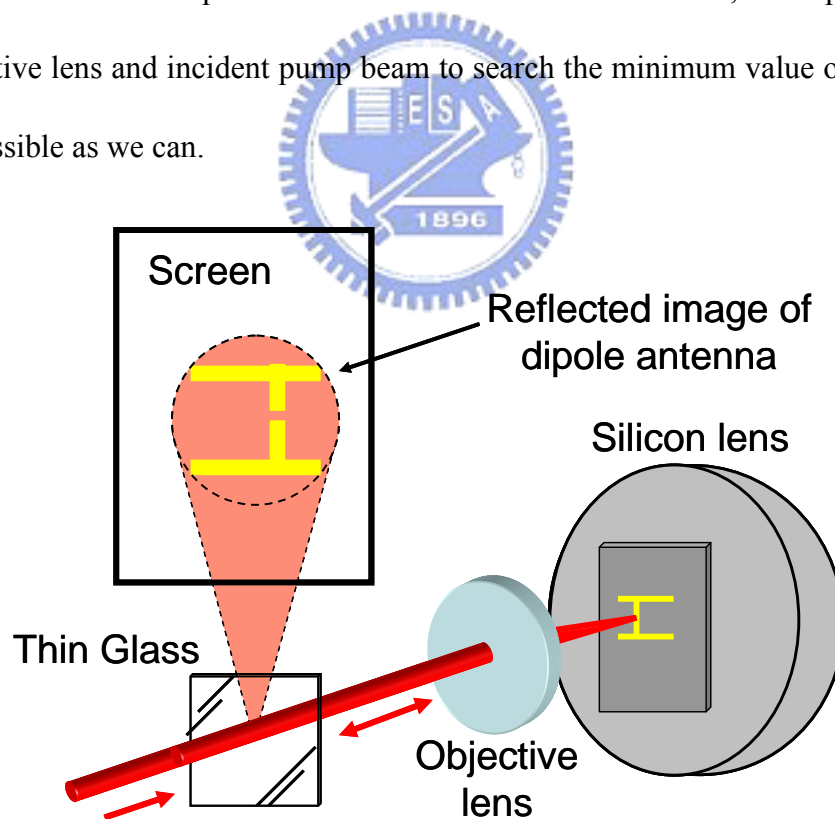


Figure 3.1-2 Schematic of focused the pump laser on the gap of dipole antennas.

3.2 Electric characteristics measurement

3.2-1 Experiment setup

In order to measuring the performance, we directly excited our PC antenna by using femto-second mode-locked Ti:sapphire laser as our source. The excitation pump pulse has a center wavelength at ~ 800 nm, ~ 50 fs (FWHM) pulse width and the repetition rate is about 82MHz. The femto-second pump pulse was focused by an objective lens on the biased gap of the PC antenna, which has put on the mount we design. The emitted THz radiation was collimated and focused by a pair of off-axis parabolic mirrors onto the detector. We used a instrument, Model 2410 High-Voltage SourceMeter, giving bias to the PC antenna and measure the current-voltage curve. To measure total THz power, we used a 4.2 K liquid-helium-cooled Si bolometer as our detector, which was carefully calibrated with a blackbody radiation source. The experiment setup for generation and detection of THz radiation is shown in Figure 3.2-1.

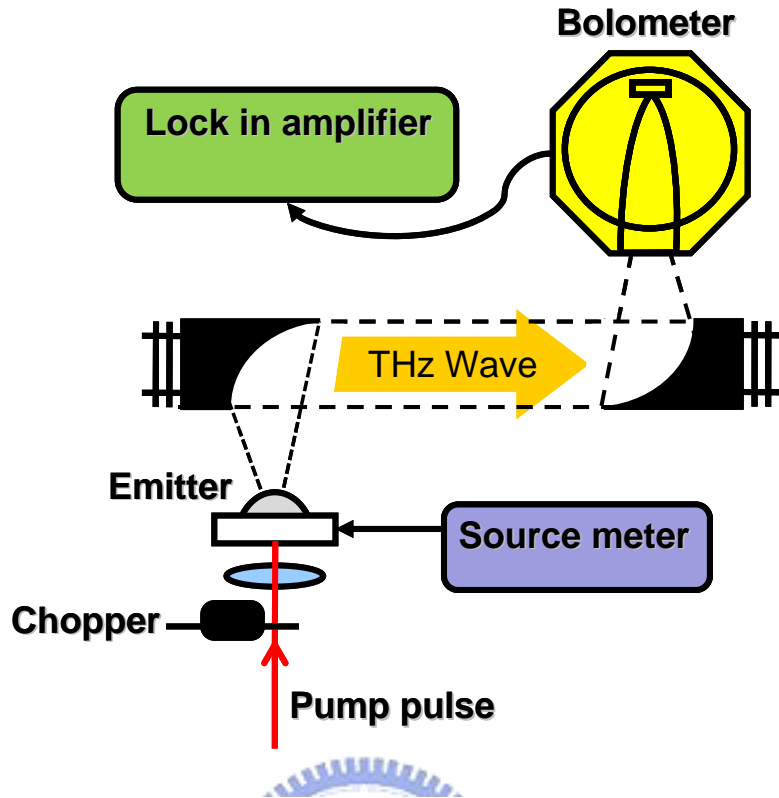


Figure 3.2-1 Schematic of experiment setup for measure the electric characteristics of PC antenna.

3.2-2 The calibration of the Si bolometer

Before using bolometer to detect THz radiation, we need to calibrate our meter firstly. The output of the bolometer is a voltage signal; it is not directly the power of the THz radiation. We use a blackbody radiation as the thermal source to radiate electric wave for the bolometer which we need to calibrate. According to the literatures [33-34], we can get the following equation (3.2-1).

$$R_{\text{peak}} = \frac{V_{\text{output}}}{\frac{A_{\text{BB}} A_{\text{d}}}{R^2} F_{\text{F}} \int_{\lambda_1}^{\lambda_2} R(\lambda) \frac{M(\lambda, T)}{\pi} d\lambda} \quad (3.2-1)$$

Where λ_1 and λ_2 are the cut-on and cut-off wavelength, which we set from $100 \mu\text{m}$ to $3000 \mu\text{m}$, in the response spectrum of our Si bolometer limited by the window filter. R_{peak} is the peak response in the response spectrum. R is the distance between the bolometer and the blackbody radiation source. A_{BB} and A_d are the area of aperture in the blackbody radiation source and the detective window of bolometer, respectively. $R(\lambda)$ is the response spectrum of the bolometer which is assumed to have a rectangle shape due to that the response of the Si bolometer is nearly independent of the frequencies from cut-on to cut-off wavelength, although the response of the Si bolometer actually decrease with the decrease of the frequency slightly. V_{output} is the voltage value which we obtain in lock-in amplifier. F_f is the modulation parameter of chopper, which is about 0.5. There is the experiment setup in Figure 3.2-2. Then, $M(\lambda, T)$ is the absolute power spectrum of the blackbody radiation source, which is the function of wavelengths and temperatures. The formula is given as following equation (3.2-2).

$$M(\lambda, T) = \frac{3.73 \times 10^4}{\lambda^5 (e^{\frac{14388}{\lambda T}} - 1)} \quad (3.2-2)$$

where the unit is $\text{Wcm}^{-1}\mu\text{m}^{-1}$. There is the experiment setup show after calibrate Bolometer, we know that the obtained response is about 50 mV per μW with the preamplifier gain set to 180 chopping frequency. So we can use the information of the voltage value we measure in experiment to calculate the energy power of THz radiation.

3.3 The time & frequency domain of THz pulse

In order to measure the time and frequency domain of THz pulse generated from PC antenna, we use two different systems for measurement; one of them is Martin-Puplett-type Fourier Transform Infrared Spectrometer (FTIR) system and the other is Terahertz Time-Domain Spectroscopy system (THz-TDS). In this section, we will introduce the setup of two different systems in detail.

3.3-1 Martin-Puplett-type Fourier Transform Infrared Spectrometer (FTIR)

Method & Setup



The design of the Martin-Puplett polarization interferometer which is based on a concept originally produced by Martin and Puplett in 1969 resembles the well-know Michelson interferometer. The Martin-Puplett polarization interferometer takes advantage of the polarization of electromagnetic radiation. In the field of THz frequency range, it is the most interferometer system is used. It has also been choice as the spectrometer in sub-millimeter wavelength range. Comparing the classical Michelson interferometer, it offers several advantages. Such as, the modulation efficiency of the polarizing beam splitter is higher and more uniform under wide spectral range. The simplified schematic is shown in Figure 3.3-1.

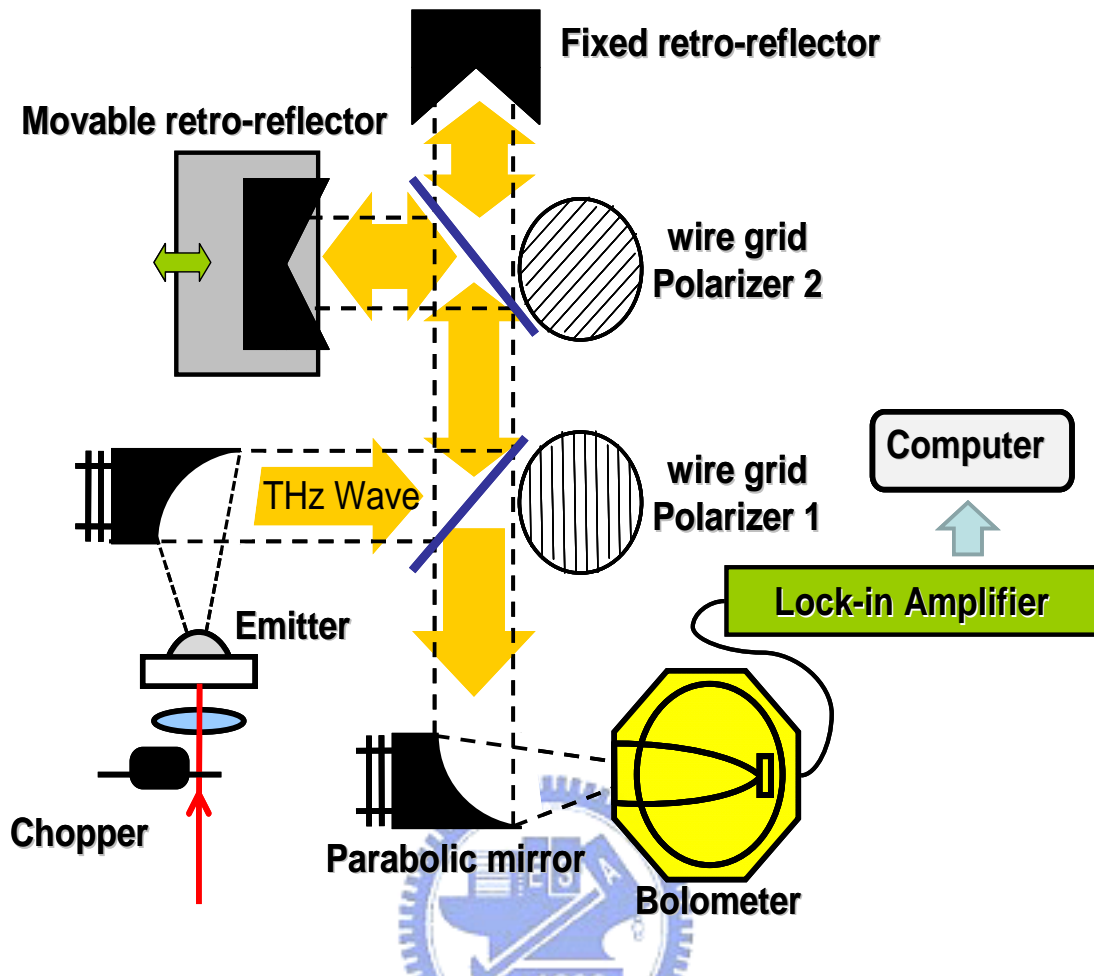


Figure 3.3-1 Schematic of a Martin-Puplett-type Fourier Transform

Infrared Spectrometer (FTIR) system

We use the parabolic mirror to collect THz radiation and become the parallel beam, then we incident the parallel beam into the Martin-Puplett polarization interferometer system. The spectrometer utilized two wire grid polarizes which will discuss clearly later, used also as the polarizing beam splitters. The reflected and transmitted waves in two arms of the spectrometer have equal intensities while their directions of polarization are orthogonal to each other. The retro-reflector in each arm rotates the polarization of the incident light 180°. The

orthogonal transmitted and reflected waves are recombined at wire grid polarizer #2, then propagated through the wire-grid polarizer #1 and be collected by a parabolic mirror. By scanning the movable retro-reflector, the interferogram can be measured by the bolometer and stored by the computer.

Wire grids

For far-infrared spectroscopy, an effective polarizer can be made from an array of closely spaced parallel metallic wires, and it is the so-called wire grid. When an incident electric field passes through the wire grid, it can be divided into one component parallel and one perpendicular to the wire. The parallel component induces a counteracting current in the metal and is thus reflected. In another part, the normal component can pass through the wire grid with a little attenuation. If the thickness d of the wires and the spacing s are small compared to the wavelength of the incident wave, the modulus of the reflection coefficients for the electric field components parallel and perpendicular to the wires can be calculated by equation (3.3-1) and (3.3-2) [35].

$$|r_{\parallel}| = \left[1 + \left(\frac{2s}{\lambda} \right)^2 \ln \left(\frac{s}{\pi d} \right)^2 \right]^{-\frac{1}{2}} \quad (3.3-1)$$

$$|r_{\perp}| = \left[1 + \frac{(2\lambda s)^2}{\pi^4 d^4} \right]^{-\frac{1}{2}} \quad (3.3-2)$$

In our experiment setup, the wire grid we used made of $10 \mu\text{m}$ thick tungsten wire wound on a circular frame placed at a distance of $45 \mu\text{m}$. The reflectivity of the electric field for these parameters is plotted in Figure 3.2-2. While the parallel

component is reflected nearly perfectly over the whole spectral range, the transmission of the normal component decreases towards higher frequencies. According the experiment result, the frequency of PC antenna we measure would not be higher than 1.5THz. So we can ignore the THz power decrease from the wire grid.

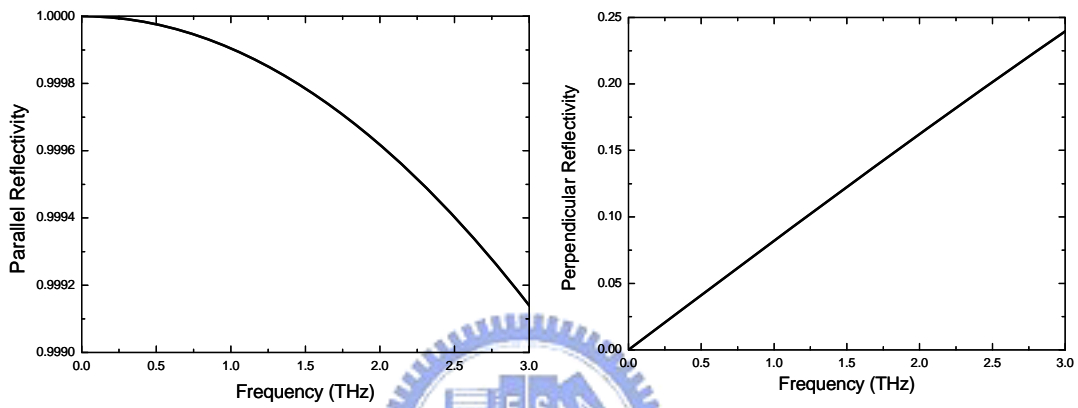


Figure 3.3-2 The reflectivity of the electric field dependent with frequency under (a) parallel and (b) perpendicular component.

3.3-2 Terahertz Time-Domain Spectroscopy (THz-TDS)

Setup

The THz time-domain spectroscopy system is shown in Figure 3.3-3. The incident pump pulse was focused by an objective lens on the biased gap of the PC antenna to generate THz radiation. The THz radiation was collimated and focused by a pair of off-axis parabolic mirror on a PC sampling detector. Which was also a PC antenna mounted on the back of a Si hemispherical lens. The PC detector was

gated by femto-second probe beam pulses that were separated from the pump beam pulses by a beam splitter, and the DC photocurrent was induced by the incident electric field of THz radiation on the PC detector. Using delaying the time of the probe pulse to the pump pulse, the time-domain waveform of the electromagnetic pulse was obtained. The time resolution was limited by the carrier lifetime of the LT-GaAs used for the PC detector. To increase the signal-to-noise ratio, the pump beam was modulated with a mechanical chopper at 1 KHz, and output signal from the PC detector was measured with a lock-in amplifier and stored by the computer.

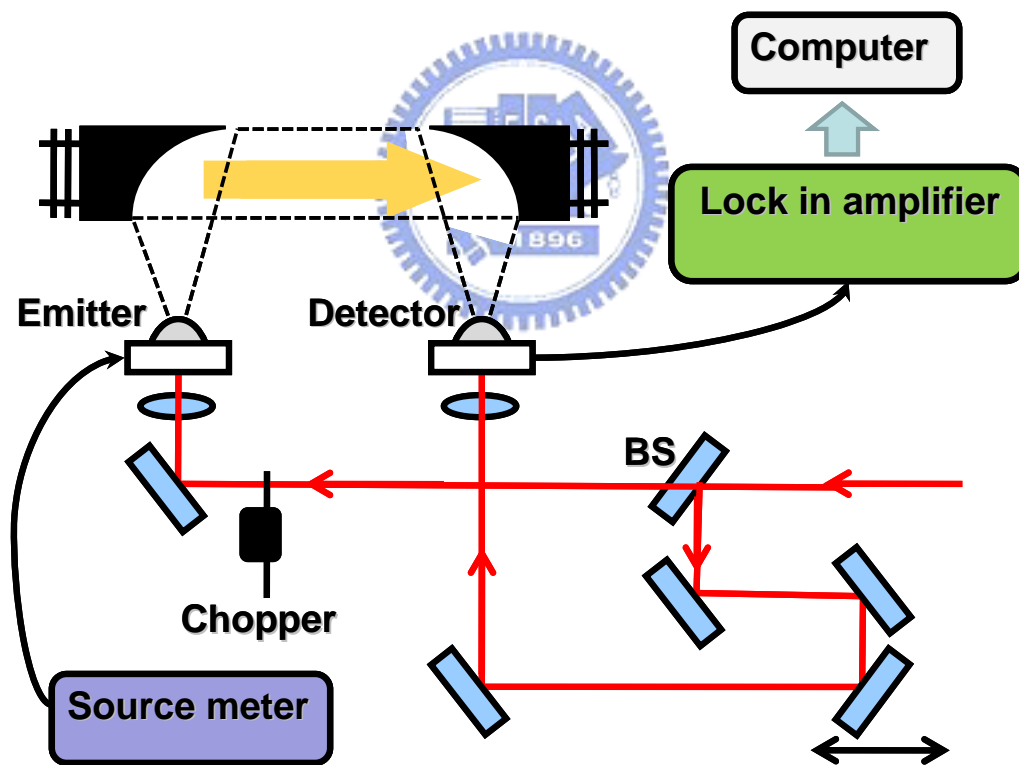


Figure 3.3-3 Terahertz Time-Domain Spectroscopy system

Chapter 4 Result and Analysis

In chapter 4, we show the experiment results of emission properties of GaAs:O PC antennas. According to the results, we analysis and discuss the results under the different conditions.

4.1 Electric characteristics result

4.1-1 Current-voltage (I-V) curve

Figure 4.1-1 shows the current-voltage characteristic result of the PC dipole antenna under different oxygen ion-implant concentration and annealing temperature, which is listed on table 3.1. We pump different incident power (25mW, 35mW, 45mW) to the PC antenna and also measure the dark current which is without pump power. It can easily confirm from Figure 4.1-1 that the I-V curve is a linear curve, the current is proportion to the bias we gave. Under the higher pump power, it can generate the more photocurrent from PC antenna. Besides, the shorter antenna length of PC antennas generates the more current than the longer antenna length of PC antennas under the same pump power and bias. We observe that the dark current of the PC antennas which have higher dosage concentration ($e14$) and annealing temperature (550°C) is lower than the PC antennas which have lower dosage concentration ($e13$) and annealing temperature (500°C).

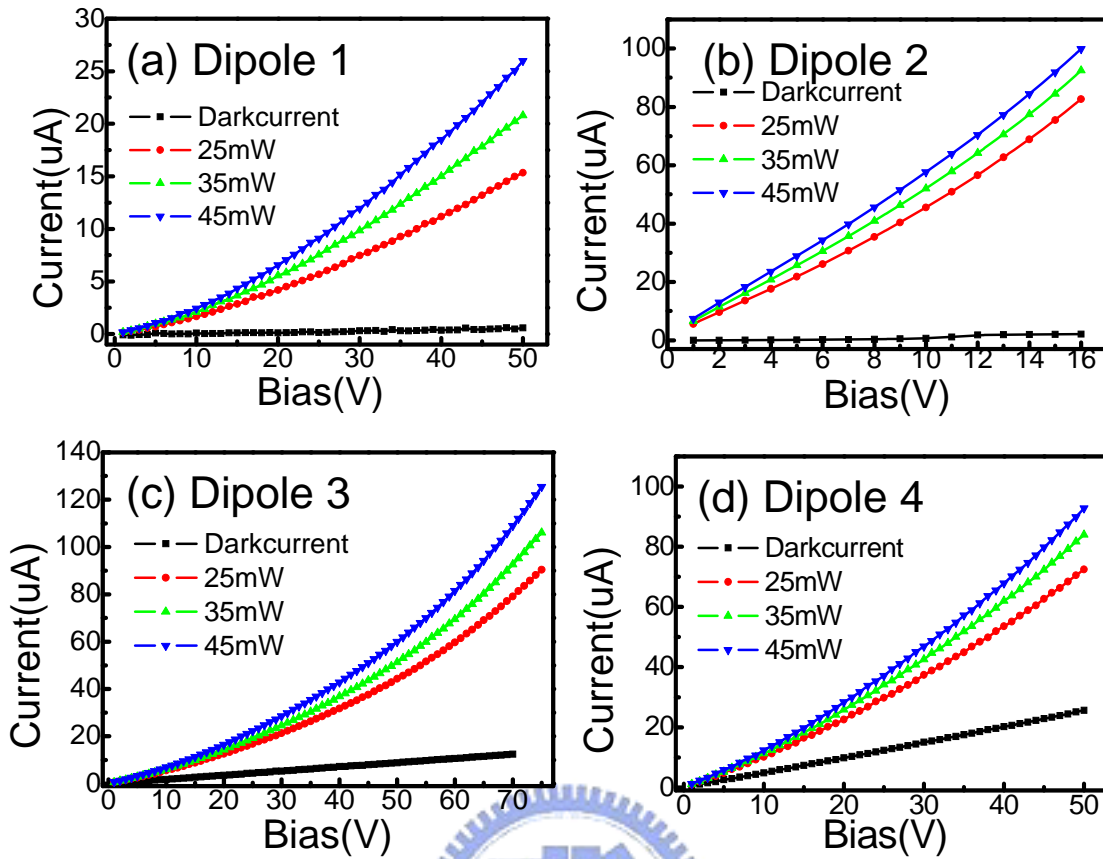


Figure 4.1-1 I-V curve of oxygen ion-implant PC antennas with different dosage concentration and annealing temperature

4.1-2 THz power-voltage curve

Figure 4.1-2 shows the bias voltage dependence of the THz absolute intensity generated from our different conditions of PC antennas with the laser beam focused near its anode under the different pump power. They are detected by the bolometer. According to the Figure 4.1-2, we can clearly obtain that the THz power increases quadratically with the bias. The higher power of THz radiation generated from oxygen ion-implant GaAs PC antenna has been demonstrated in Figure 4.1-2 (c). It is almost up to 3.5V under the high bias (70V) and pump

power (45mW).

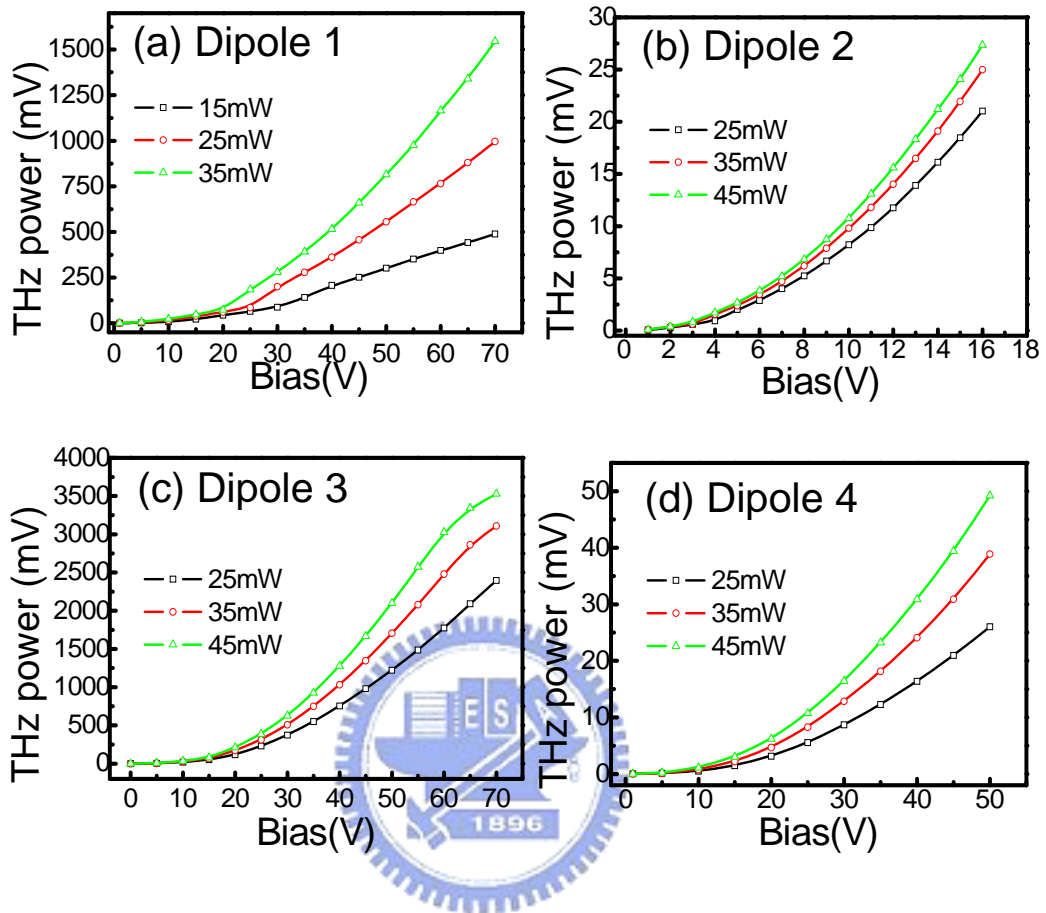


Figure 4.1-2 THz power-voltage curve of oxygen ion-implant PC antennas with different dosage concentration and annealing temperature

4.1-3 Analysis and Discussion

Figure 4.1-3 shows the bias voltage dependence of the THz intensity measured for our PC antennas using a constant pump power of 35mW. According to the result, we can observe that the lower dosage concentration of PC antenna in the same antenna length (100um) can get the higher THz power. Under the same substrate, the longer antenna length emitted higher power as expected from

Equation (2.1-38) (radiation power is proportional to the effective antenna length); the emission power of dipole3 and 4 was 1032mV and 24.09mV under the same pump and bias conditions (35mW and 40V), respectively. It is the same results using the dipole1 and 2. A higher breakdown voltage characteristic is a factor of merit for high-power THz radiation sources. However, under the high bias voltage of 70V, we didn't find the breakdown voltage threshold in dipole 1 and 3.

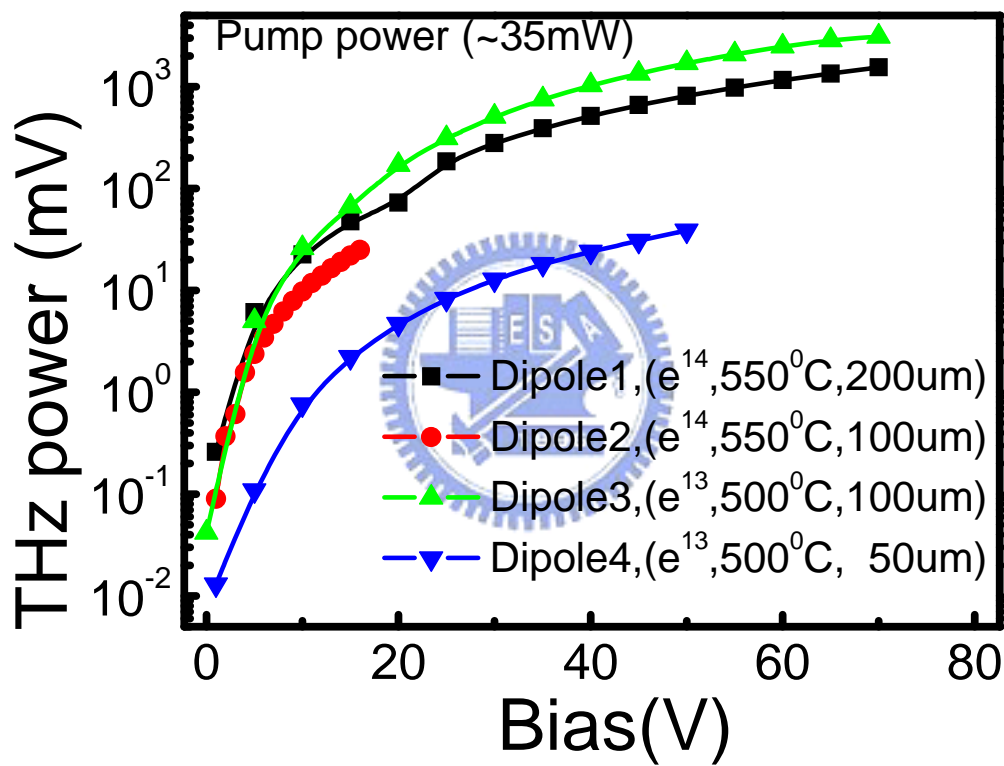


Figure 4.1-3 Intensity of THz radiation measured as a function of the bias voltage for the GaAs:O PC antenna with different conditions. The pump power is fixed at 35mW.

Figure 4.1-4 shows the pump power dependence on the intensity of THz power from the GaAs:O PC antennas under constant bias voltage of 15V and the same structure, respectively. Dipole3 of PC antenna which has lower dosage

concentration and lower annealing temperature can excite the higher power than Dipole2. We can observe a saturation regime which occurs at excitation powers greater than about 45mW. This phenomenon originates from the screening of the local bias field by the photocarriers generated in the gap between of our antenna electrodes. This effects were discussed by Benicewicz et al. [36], and Darrow et al. [37] for large-aperture PC antennas. The same discussion can also be applied to the case of small gap PC antennas by taking into account the effect of the nonuniform spatial radiation pattern of a dipole antenna, which only gives rise to a difference by a constant factor in the radiation efficiency [12].

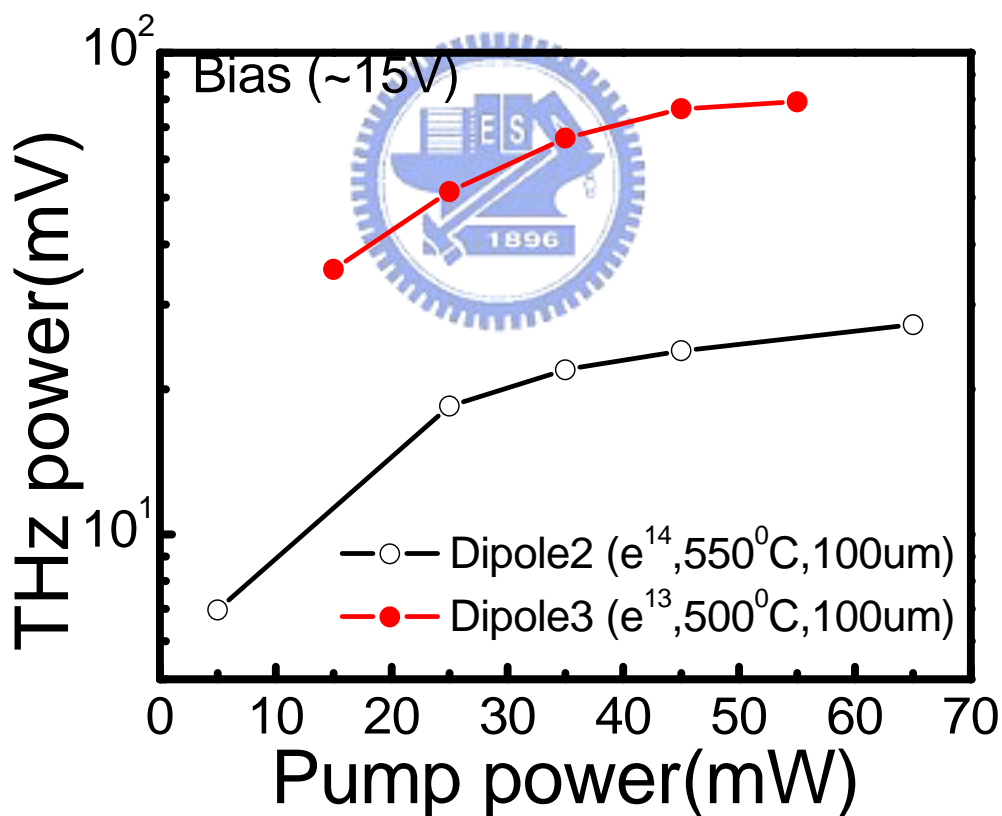


Figure 4.1-4 Intensity of THz radiation measured as a function of the laser pump power for the GaAs:O PC antenna under the same antenna length. The bias is fixed at 15V.

4.2 THz wave from of GaAs:O antennas

4.2-1 Measurement result

Martin-Puplett polarization interfered Spectrometer (FTIR)

We chose the two antennas dipole1 and dipole3 as our THz emitters which have different condition to measure the time and frequency domain by using FTIR system. The step of each signal in time domain is $20\ \mu\text{m}$, it is equal to the time resolution which is about 66.7 femto-second. The results of spectrum are shown in Figure 4.2-1 (a) and (b). The insets in Figure 4.2-1 (a) and (b) show the time domain of antennas detected by FTIR system. We observe that the bandwidths of dipole1 and dipole3 were about 0.6 THz and 0.8 THz. However, the signal-to-noise ratio of the spectrum measured by FTIR system is only 100:1. It is because that the SN rate needs to consider the limited of bolometer. Besides, THz radiation needs to propagate the farther distance and it is easily absorbed by atmosphere to loss the signal of higher frequency. As this result, we need to use another THz system which has higher SN rate to measure the precise data.

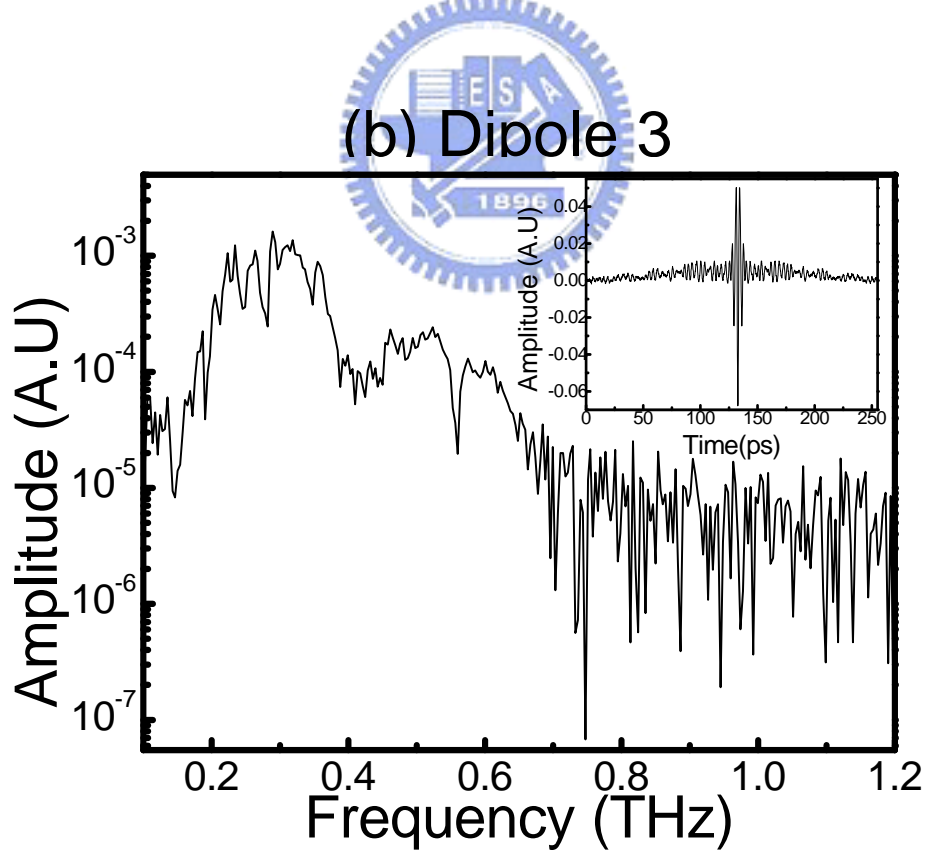
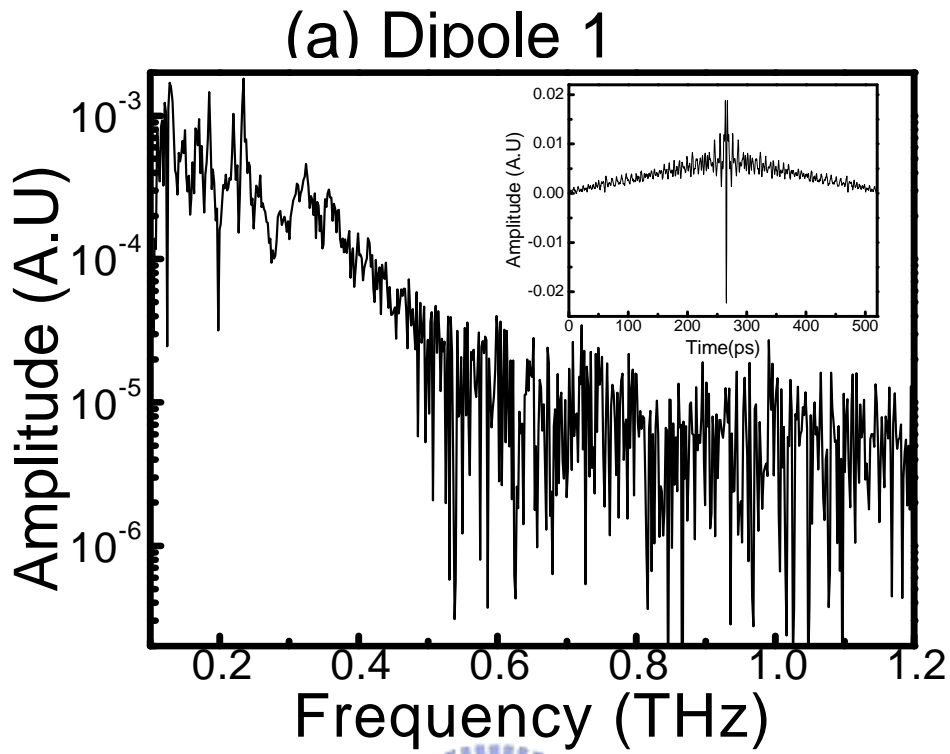


Figure 4.2-1 The spectrum of different PC antennas (a) dipole 1 (b) dipole 3.

The inset is the interfere waveform measured by FTIR system.

Terahertz Time-Domain Spectroscopy (TDS)

We use the dipole 1 as our THz emitter to be measured by TDS. The THz wave forms emitted from Dipole 1 is shown in Figure 4.2-2. We pump different incident power (35, 45, and 55mW) under the constant bias 40V shown in Figure 4.2-2(a) and applied various bias voltages (20, 40, and 60V) with the same pump power 35mW shown in Figure 4.2-2(b), respectively. And the spectrum of THz wave under the different conditions are shown in Figure 4.2-2(c) and (d). We observe that the peak of THz wave form increase with bias and pump power.

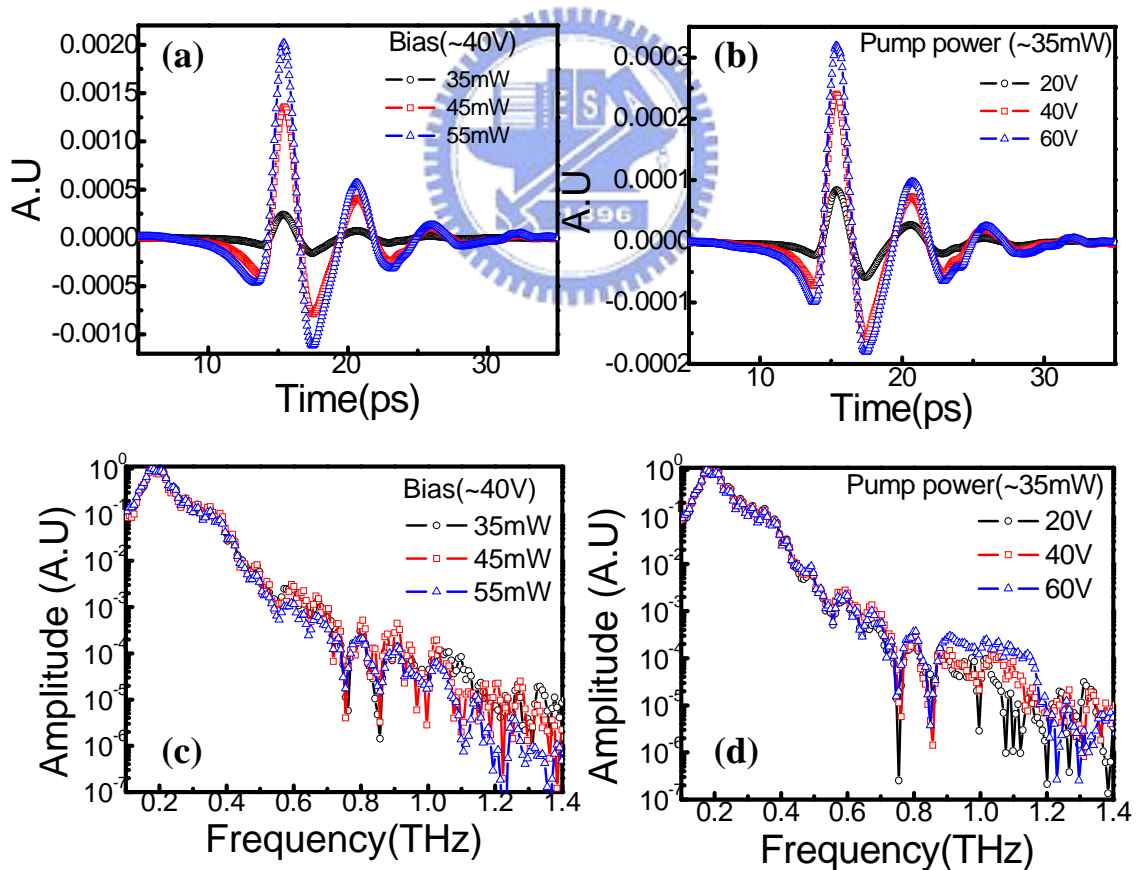


Figure 4.2-2 THz wave forms and spectrums of dipole 1 under (a) & (c) the different pump power and (b) & (d) the different bias.

However, we didn't find the phenomenon which the positive main peak shifts slightly to the earlier time delay with the increase in bias in the material of GaAs:O of PC antenna or the spectrum shift to higher frequency, which this phenomenon has been record in literature [17].

In other PC antenna, it can measure the same phenomenon as Dipole 1. Besides, we also observed the breakdown voltage thresholds by using TDS system. In Dipole 3 of PC antenna, the bias dependence of the amplitude at the positive main peak is shown in Figure 4.2-3. Under the same pump power (~55mW), the GaAs:O antenna showed a high breakdown voltage threshold (>110 kV/cm). The higher breakdown voltage is an advantage of GaAs:O antennas.

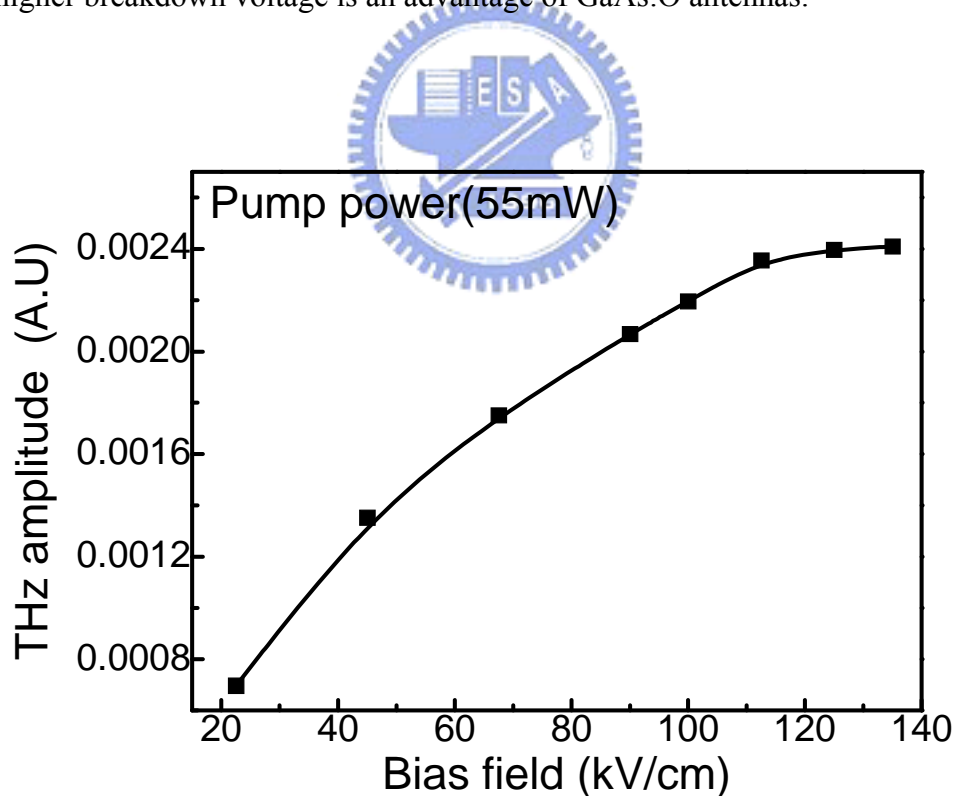


Figure 4.2-3 The bias dependence of amplitude at the positive main peak in Dipole 3 under the same pump power.

We measured the spectrum of our PC antenna and the Figure 4.2-4(a) and (b) show the spectrum of Dipole 1 and Dipole 3. The spectral distribution of Dipole1 is centered at near 0.2 THz and Dipole 3 is about 0.25 THz. According to the literature [32], the resonant frequency ν_r of a dipole antenna on the thick dielectric substrate can be approximated as

$$\nu_r = \frac{c}{\lambda_r} = \frac{c}{2l_e \varepsilon_e^{1/2}} = \frac{c}{2l_e [(1+\varepsilon_d)/2]^{1/2}} \quad (4.2-1)$$

where λ_r is the resonance wavelength, ε_e and ε_d are the effective dielectric constant defined by $\varepsilon_e = (1+\varepsilon_d)/2$ and the dielectric constant of the substrate (for GaAs $\lambda_r = 13$ in THz frequencies [32]), respectively. There are some ambiguities in defining the effective length because of the finite antenna width and the continuous connection of the dipole edge to the coplanar transmission line. We assume the diagonal length of the antenna structure including the width of the coplanar transmission line ($= \{(L+2D)^2 + W^2\}^{1/2}$) as the effective length of the antennas, the resonant frequency can be calculated as 0.23 and 0.37 THz for Dipole1 and 3, respectively. We expect that the actual resonance frequency can be observed in our result. The resonance frequency should be shifted for different antenna dimensions. According to the results, it can be observed the peaks of spectrums under the lower frequency. we can attribute to the resonance frequency. Because of it, the amplitude of THz radiation under the higher frequency is independent on antennas structures. It is dependent on the properties of substrate material.

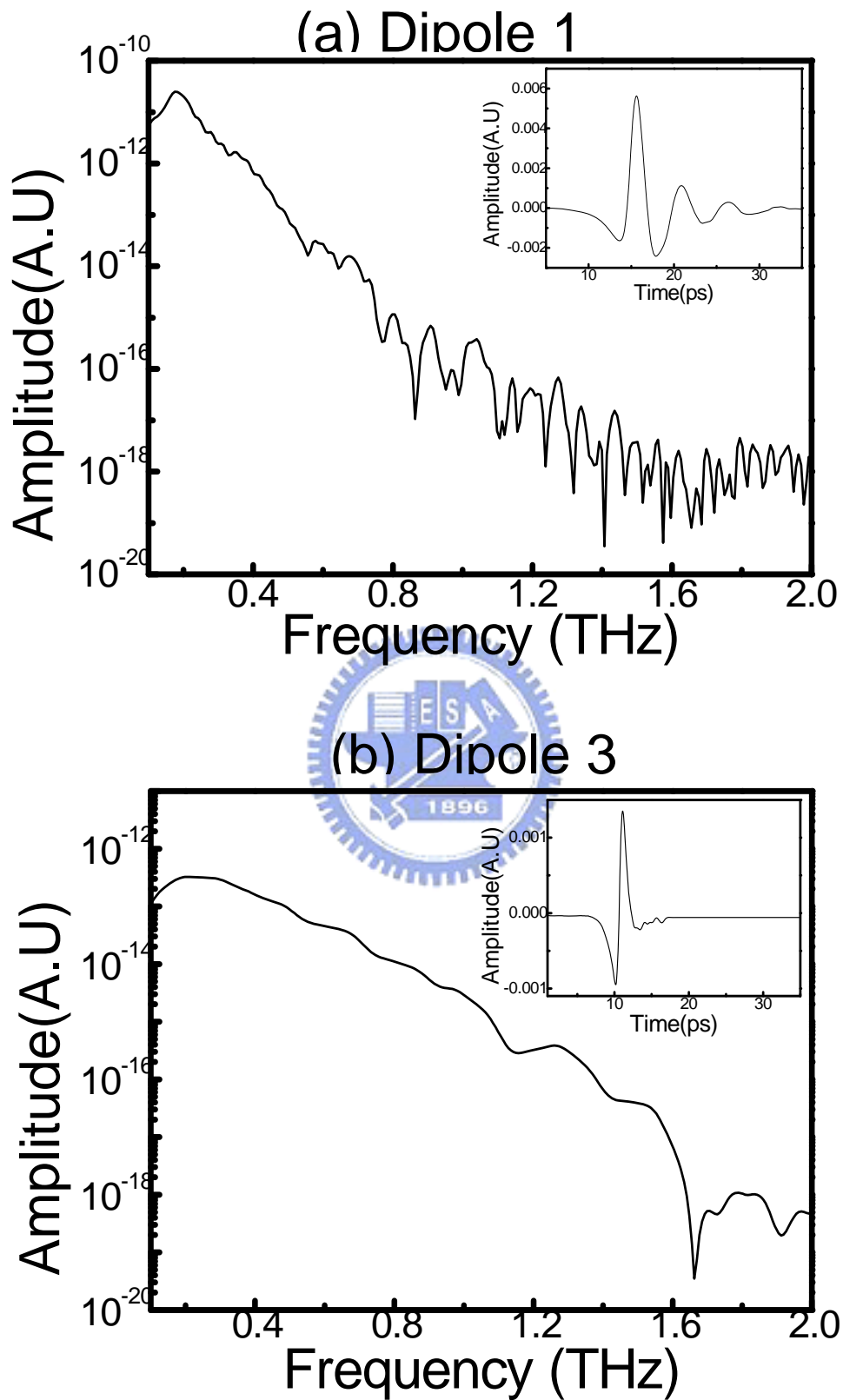


Figure 4.2-4 The spectrum of different PC antennas (a) dipole 1 (b) dipole 3.

The inset is waveform of electric pulse measured by TDS.

4.2-2 Different systems (FTIR & TDS)

According to the result of Chapter 3, the spectrums of GaAs:O PC antenna with different material conditions have been measured by two systems, Martin-Puplett-type Fourier Transform Infrared Spectrometer (FTIR) and Time domain system (TDS). Then, we normalized the data to compare the result with different measurement way. The spectrum of Dipole 1 and 3 which is compared with different measurement systems are shown in Figure 4.2-5(a) and (b). From the results, we can clearly observe that the signal-to-noise (SN) ratio in TDS ($\sim 10^7:1$) is much better than in FTIR ($\sim 100:1$). The SN ratio of FTIR is limited by bolometer, which has been discussed in section 4.2-1. In the lower frequency range (from 0.1 to 0.6 THz), the curve of spectrum is similar in different measurement way. However, because of the higher SN ratio in TDS, we can easily observe the signal of high frequency (over 0.6 THz) and get clear broader bandwidth of PC antenna. In FTIR, the power of signal in high frequency is the same as the background noise.

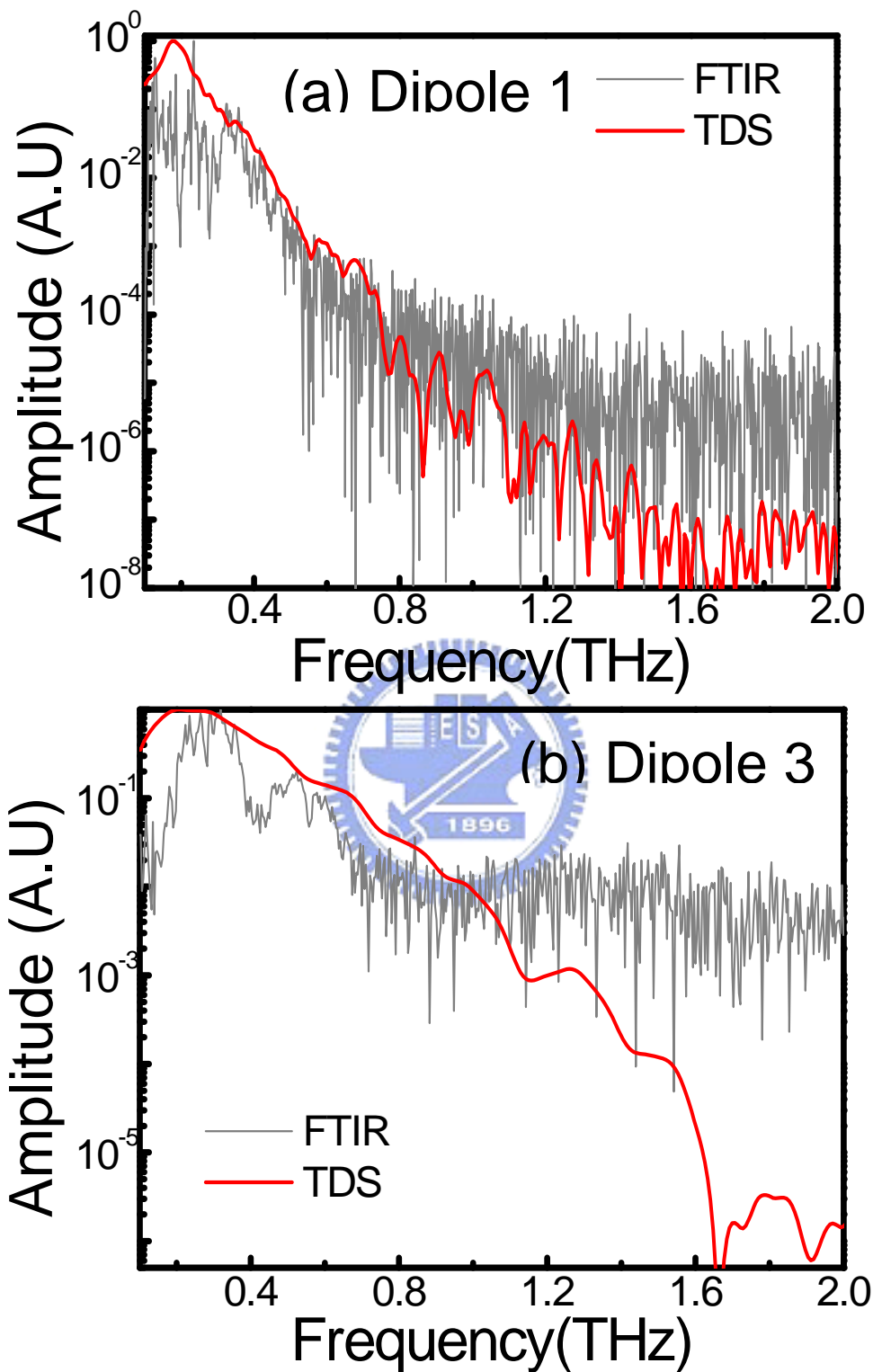


Figure 4.2-5 The comparison of spectrum with different measurement system

in antenna of (a) Dipole 1 and (b) Dipole 3.

4.2-3 Analysis and Discussions

THz wave form

The THz wave form emitted from the GaAs:O (solid curve) and LT-GaAs (open circles) dipole antenna measured by TDS are shown in Figure 4.2-6. Each THz wave form was normalized at its main peak amplitude. We can observe a clear different curve emitted from different antennas. To explain the observed difference in the wave forms of the THz radiation emitted from the different antennas, we need to consider the carrier dynamics in photoconductive substrate.

To interpret the THz radiation wave form, we use the dipole radiation approximation, where the emitted field is assumed to be proportional to the time derivative of the transient current $J(t)$ at far field. In this approximation the main (positive) peak observe in wave forms in Figure 4.2-6 is attributed to the rises of the surge current by photo-carrier injection and subsequent carrier acceleration under the bias field in the PC antennas, whiled second negative peak preceded by the main peak is attributed to the decay of the current governed by the carrier trapping time [17]. If we assume that the current rise is determined by the pump laser pulse width (~ 80 fs), the carriers contribute to the current rise in the same way. However, the carrier trapping time is different in substrate of each antenna. From the result, we can find that the LT-GaAs has the shortest carrier decay time (< 1 ps) and the substrate GaAs:O (e^{13} & 500°C) (~ 1.5 ps) is shorter than GaAs:O (e^{14} & 550°C) (~ 2 ps). Reduction of the carrier lifetime contributes to enhance the

content of high-frequency Fourier components present.

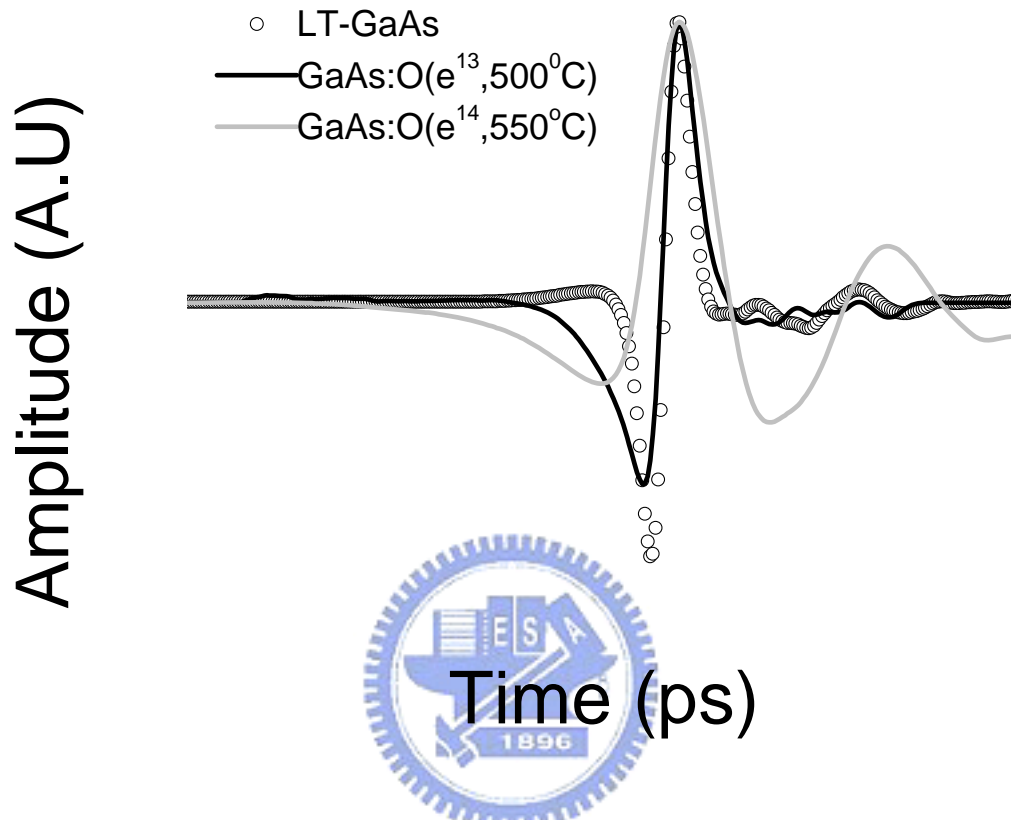


Figure 4.2-6 The THz wave form of the GaAs:O PC antenna under the different conditions and compared with LT-GaAs PC antenna.

Spectrum

Figure 4.2-7 shows the spectrums of GaAs:O PC antenna Dipole 1 and Dipole 3. From the result, we can find that one of our PC antennas Dipole 3 and 4 which the multi-implants dosage concentrations are 2.5×10^{13} ions/cm² (500Kev & 800Kev) and 4×10^{13} ions/cm² (1200kev) and the annealing temperature is 500°C for 60s have broader bandwidth (~1.6 THz). However, the spectrum of

another PC antennas Dipole 1 and 2 which the multi-implants dosage concentrations are 6×10^{13} ions/cm² (500Kev & 800Kev) and 1×10^{14} ions/cm² (1200kev) and the annealing temperature is 550°C for 60s are not broader (~0.8 THz). According to the Figure 4.2-7, the THz power of Dipole 1 is just concentrated in the lower frequency (~0.2 THz) even though it can get higher SN ratio of spectrum than Dipole 3.

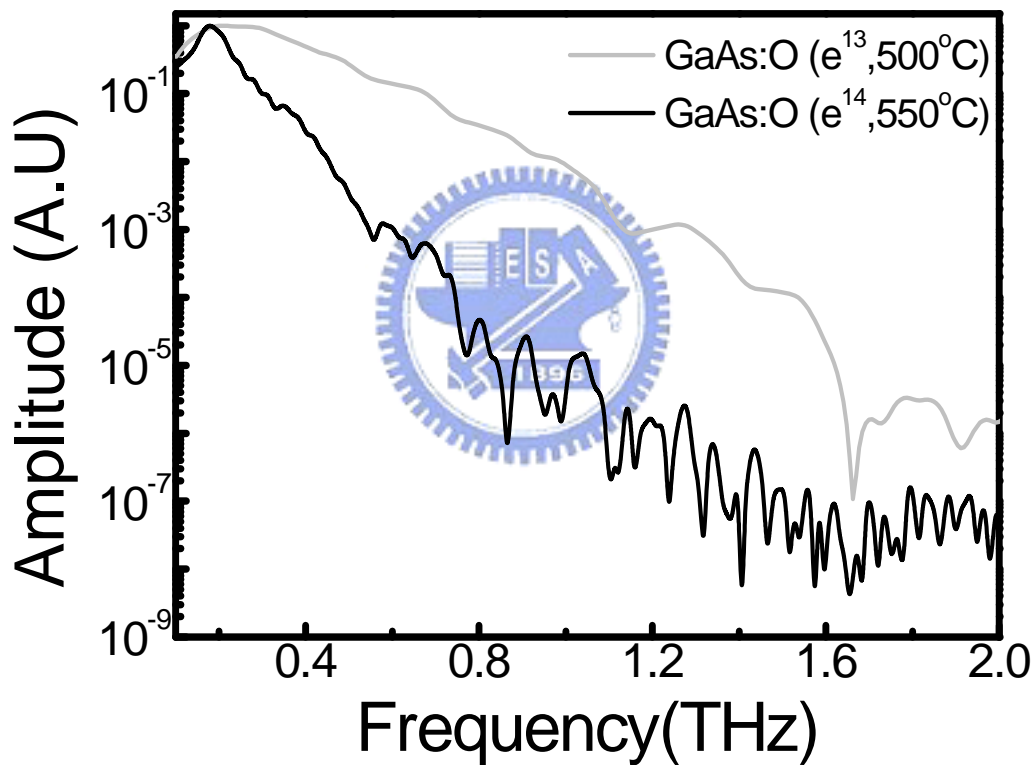


Figure 4.2-7 The spectrum of the GaAs:O PC antenna under the different conditions.

4.3 Compare with LT-GaAs antenna

According to the results in section 4.2-3, we have demonstrated that GaAs:O

PC antenna can achieve broader bandwidth of spectrum (~ 1.6 THz) . So we tried to compare with the material of Low-temperature (LT) grown GaAs which has widely been used as PC antennas. The first step, we fabricated the same structure of dipole antenna as LT-GaAs PC antenna which has been used in our lab, to study the different of emission properties in GaAs:O and LT-GaAs PC antenna. The detail antenna structure is shown in Figure 4.3-1, which the antenna length is $30\ \mu\text{m}$ and the gap is only $5\ \mu\text{m}$. In this part, we compared the current, THz power and spectrum with two different materials using as the substrate of antenna.

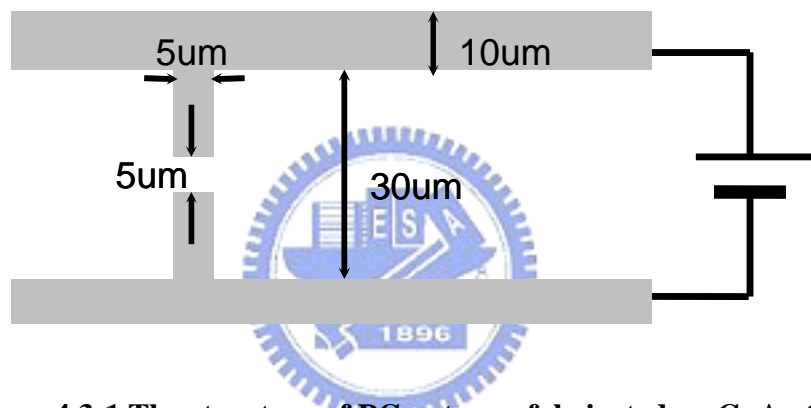


Figure 4.3-1 The structure of PC antenna fabricated on GaAs:O and LT-GaAs material

4.3-1 Electric characteristics

The result of bias dependent with total current and THz power are shown in Figure 4.3-2 (a) and (b). In Figure 4.3-2 (a), we compared the current with different material under the same pump power ($\sim 35\text{mW}$) and measured dark current of each material. Although the dark current of LT-GaAs material is lower than GaAs:O and the current measured from LT-GaAs is higher than GaAs:O under the lower bias ($< 15\text{V}$). However, when the bias is greater than 15V , we can

obtain that the current generated from GaAs:O PC antenna is higher. And the photocurrent of GaAs:O material is about 0.03 mA which is more than LT-GaAs (~0.02 mA). Because of it, we measured the THz power generated from two kinds materials of PC antenna by bolometer and the result is shown in Figure 4.3-2 (b). According to the equation (2.1-38) which has discussed before, the power of THz

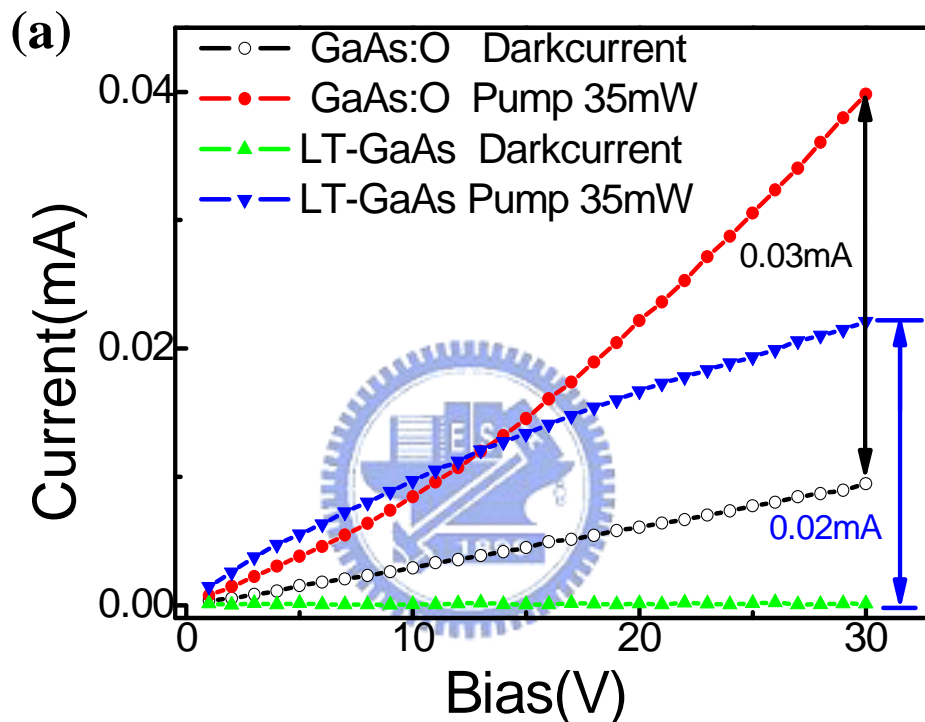


Figure 4.3-2 (a) Current-voltage curve measurements for GaAs:O and LT-GaAs PC antenna with pump power (~35mW) and without laser irradiation.

radiation is proportion to the photocurrent (the effect length is the same). In the same pump power (~35mW), the THz power generated from GaAs:O PC antenna increases quadratically with the bias under the higher biases. And we obtained that the THz power of generated from LT-GaAs PC antenna only increases with factor

$V^{1.4}$. As the result, we has demonstrated that the GaAs:O PC antenna can generate the higher THz power ($\sim 8.42\text{mV}$) than the LT-GaAs PC antenna ($\sim 4.74\text{mV}$) under the high bias. It is almost two times for the GaAs:O emitter than for the LT-GaAs emitter.

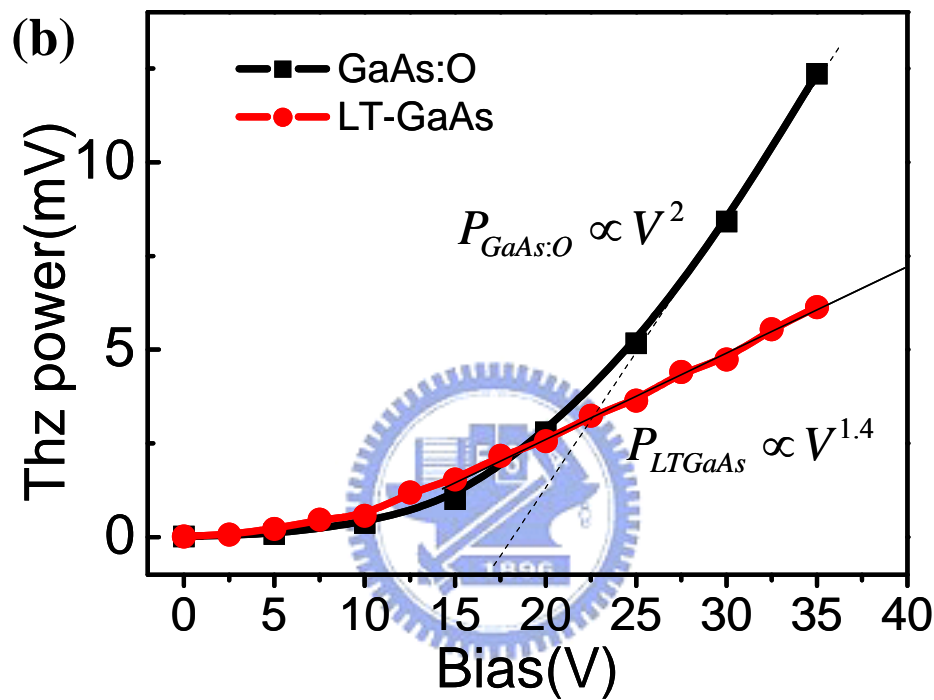


Figure 4.3-2 (b) THz power generated from GaAs:O and LT-GaAs PC antenna versus bias voltage under the same pump power ($\sim 35\text{mW}$).

4.3-2 THz wave form & Spectrum

We also used the time domain system which has described above to measure the THz wave form and spectrum, to compare the emission properties with two different materials of PC antenna.

THz wave form

Figure 4.3-3 shows the result of THz electric pulse of GaAs:O PC antenna in time domain. We used the different pump power and bias to observe the variation of THz wave form. In Figure 4.3-3 (a), we tried to pump the different incident power (35, 45, and 55mW) under the same bias ($\sim 25\text{V}$) and obtain the phenomenon of THz electric pulse changing in time domain. And we changed the bias (15, 25, and 30V) under the same pump power ($\sim 45\text{mW}$) which is shown in Figure 4.3-3 (b). From the result, it can observe that the peak of THz pulse is increased apparently by applying the higher bias.

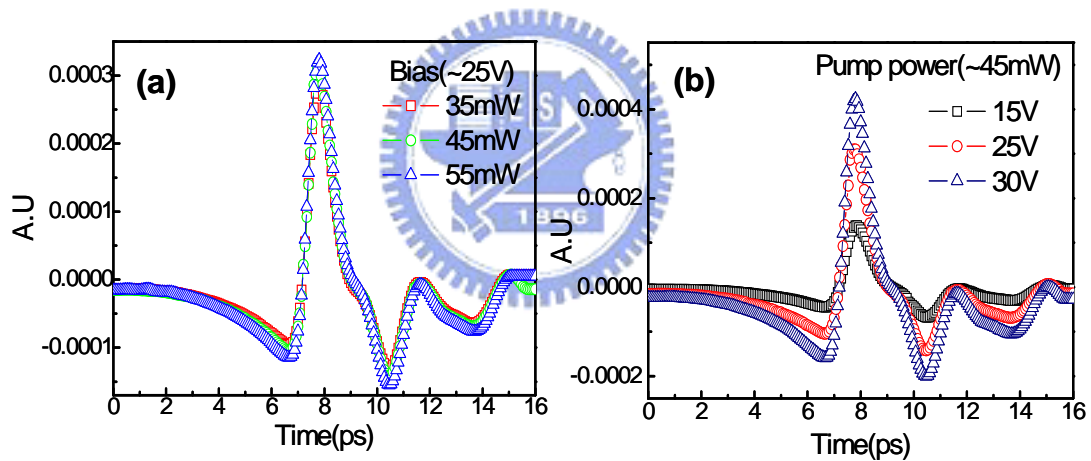


Figure 4.3-3 THz wave form of GaAs:O PC antenna under (a) the different pump power and (b) the different bias.

Spectrum

The Fourier transform spectrum of the THz wave form is shown in Figure 4.3-4. And it compared with the LT-GaAs PC antenna which is the same structure. We expect that the bandwidth of our GaAs:O PC antenna can be approximate to the

LT-GaAs PC antenna. In Figure 4.3-4, it indicates that the THz power emitted from GaAs:O PC antenna concentrates on low frequency. Under the lower frequency range (<0.3 THz), the amplitude of GaAs:O is higher than LT-GaAs. However, the bandwidth of GaAs:O PC antenna can attain to about 1.5 THz which is not broader than LT-GaAs PC antenna (~2 THz) in our experiment. According to the equation 4.2-1, the resonant frequency ν_r of this dipole antenna can be calculated as 1.13 THz. But we also didn't clearly find such resonance peaks at the expected resonant frequency. According to the equation 4.2-1, we did not clearly

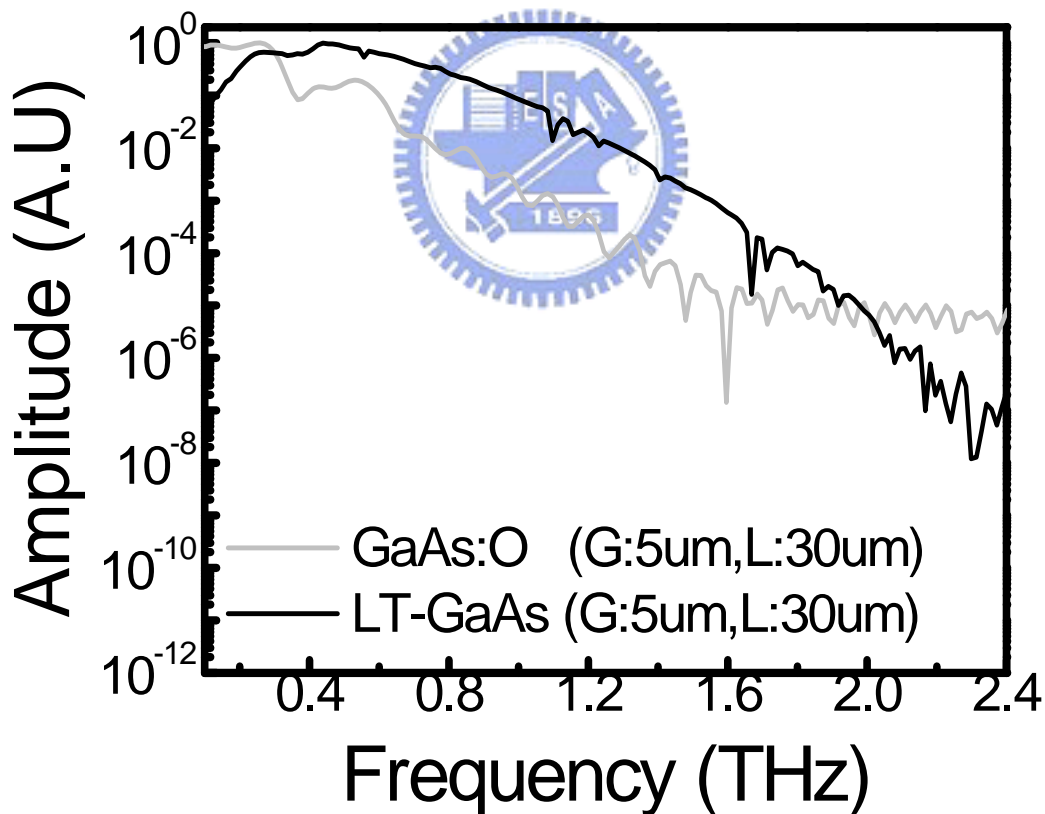


Figure 4.3-4 The spectrum of dipole antenna with different substrate GaAs:O and LT-GaAs.

find resonance peaks at the expected frequency ($\sim 1.13\text{THz}$), nor peak shifts of spectral distributions for different dipole antenna lengths. It maybe can attribute this to the slow decay time of the photocurrent limiting the generation of the higher frequency components of radiation, or it is attributed to other factors, such as the broadening of the resonance peak as a result of the large antenna width or the damping of the switching response because of the capacitance of the photoconductive gap at high frequencies.



Chapter 5 Conclusion

In the last chapter, we conclude the results of emission properties and list some works about Oxygen ion-implanted GaAs PC antennas which can be researched in the next step.

5.1 Summary

We have demonstrated that the THz radiation generated from Oxygen ion-implanted GaAs with dipole antenna device. In our study, the main point is to compared the emission properties of Oxygen ion-implanted GaAs under different multi-implants dosage concentrations (2.5×10^{13} ions/cm² (500 keV & 800 keV), 4×10^{13} ions/cm² (1200 keV) and 6×10^{13} ions/cm² (500 keV & 800 keV), 1×10^{14} ions/cm² (1200 keV) and annealing temperature (550°C and 500°C for 60s).

In the result of electric characteristics, the current-voltage and THz power-voltage curve are measured. The results show that this kind of material is suitable for high power THz radiation generation. The GaAs:O PC antenna (1×10^{13} , 500°C) can get more than 3.5V which the energy power is equal to $70 \mu\text{W}$ under applying 70V dc bias and 45mW pump power. Besides, the advantages of the GaAs:O PC antennas which are the high breakdown voltage threshold biasing (~ 110 KV/cm) and large saturating optical pumping power (~ 40 mW) are observed from our experiments. We also compared the different antenna length (200, 100,

50um). It can be observed that the longer antenna length emitted higher THz power (radiation power is proportional to the effective antenna length and photocurrent).

In the result of THz time and frequency domains, we measured the THz radiation wave forms of GaAs:O PC antennas with FTIR and time-domain systems. The broader bandwidth which is about 1.5 THz is obtained for these ion-implanted devices (e13, 500°C).

We also compared the material of GaAs:O (e13, 500°C) with LT-GaAs under the same structure of dipole antenna. By using bolometer, the THz power we measured is almost 2 times higher for the GaAs:O emitter ($\sim 0.17\mu\text{W}$) than for the LT-GaAs emitter ($\sim 0.09\mu\text{W}$) under the same pump power ($\sim 35\text{mW}$) and dc bias ($\sim 30\text{V}$). Although the frequency of GaAs:O is not broader enough than LT-GaAs, but it could be improved by optimizing the implant dosage and annealing temperature, and adopting other antenna structures for high frequency purpose. With the higher bias field and larger pumping power confirmed in this study, GaAs:O is promising as the substrate of the PC emitter antennas for THz radiation.

5.2 Future work

We have successfully found some characteristics of the multi-GaAs:O PC antenna in the thesis. According to the property of higher output THz power, it is suitable to use as an emitter which can generate CW THz radiation by using

photomixing process. It will be researched in next step. In the result of THz frequency domains, the bandwidth of GaAs:O antennas is not broader than LT-GaAs. But it can be improved by optimizing the conditions of implant dosage and annealing temperature for high frequency purpose, or we can try to adopt other antenna structures to increase the bandwidth. Besides, the material of multi-GaAs:O needs to be measured by femto-second pump-probe system for study the carrier dynamics. We can calculate the exact carrier life time of material which can help us to improve the emission properties.



References

- [01] Matthew C. beard, Gordon M. Turner, and Charles A. Schmuttenmaer, "Terahertz Spectroscopy" J. Phys. Chem. B, **Vol.106**, pp. 7146-7159, June. (2002)
- [02] S. Mickan, D. Abbott, J. Munch, X. C. Zhang, T. van Doorn, "Analysis of system trade-offs for terahertz imaging" Microelectronics Journal, **Vol.31**, pp. 503-514,(2000)
- [03] Sang-Gyu Park, M. R. Melloch, and A. M. Weiner, "Comparison of terahertz waveforms measured by electro-optic and photoconductive sampling" Appl. Phys Lett. **Vol.73**, pp. 3184-3186,(1998)
- [04] Justin T. Darrow, Xi-Cheng Zhang, David H. Auston, Jeffrey D Morse," Saturation properties of large aperture photoconducting antennas" IEEE J. Quantum electron, **Vol.28**, no.6, pp.1607-1616,(1992)
- [05] D. H. Martin, and E. Puplett, "polarized interferometric spectrometry for the millimeter and submillimetre spectrum" Infrared Physics, **Vol.10**, pp. 105-109, (1969)
- [06] O. Morikawa, M. Tonouchi, and M. Hangyo, "sub-THz spectroscopic system using a multimode laser diode and photoconductive antenna" Appl. Phys. Lett., **Vol.75**, No. 24, pp. 3772-3774,(1999)
- [07] S. kono, M. Tani and K. Sakai, "Coherent Detection of mid-infrared radiation up to 60THz with an LT-GaAs photoconductive antenna" IEE, Proc-optoelectron, **Vol.149**, No. 3, pp. 105-109, (2002)
- [08] Sang-Gyu Park, Michael R. Melloch, and Andrew M. Weiner, "Analysis of Terahertz Waveforms Measured by Photoconductive and electrooptic sampling" IEEE J. Quantum Electronics. **Vol.35**, No. 5, pp. 810-819,(1999)

- [09] S Kono, Masahiko Tani, and Kiyomi Sakai, "Ultrabroadband photoconductive detection: comparison with free space electro optic sampling" Appl. Phys. Lett., **Vol.79**, No. 7, pp. 898-900, (2001)
- [10] Sang-Gyu Park, M. R. Melloch, and A. M. Weiner, "Comparison photoconductive sampling" Appl. Phys Lett., **Vol.73**, pp. 3184-3186,(1998)
- [11] Smith. F.W. Smith, F. W.; Le, H. Q.; Diadiuk, V.; Hollis, M. A.; Calawa, A. R.; Gupta, S.; Frankel, M.; Dykaar, D.R., "Picosecond GaAs-based photoconductive optoelectronic detectors." Appl. Phys. Lett. **Vol.54**, 890 (1989)
- [12] M. Tani, K. Sakai, and H. Mimura, "Ultrafast Photoconductive Detectors Based on Semi-Insulating GaAs and InP" Jpn. J. Appl. Phys., Part2, **Vol.36**, L1175 (1997)
- [13] D. C. Look, Thin Solid Films 231, 61 (1993)
- [14] C. Ludwig and J. Kuhl, "Studies of the temporal and spectral shape of terahertz pulses generated from photoconducting switches."Appl. Phys. Lett. **Vol.69**, 1194,(1996)
- [15] S. Kono, M. Tani, And K. SaKai, "Ultrabroadband photoconductive detection: comparison with free-space electro-optic sampling" Appl. Phys. Lett., **Vol.79**, No.7, pp. 898-900, (2001)
- [16] A. Claverie, F. Namavar, and Z. Lilorntal-Weber, "Formation of As precipitates in GaAs by ion implantation and thermal annealing."Appl. Phys. Lett. **Vol.62**, 1271,(1993)
- [17] Liu T-A, Tani M and Pan C-L "THz radiation emission properties of multienergy arsenic-ion-implanted GaAs and semi-insulating GaAs based photoconductive antennas" J. Appl. Phys. **Vol.93**, 2996,(2003)
- [18] Lin G-R, and Pan C-L "Characterization of optically excited terahertz radiation from arsenic-ion-implanted GaAs" Appl. Phys B **Vol.72**, 151,(2001)
- [19] Lloyd-Hughes J, Castro-Camus E, fraser M D, Jagadish C and Johonston M B Phys. Rev. B 70 235330,(2004)

- [20] Liu T-A, Tani M, Nakajima M, Hangyo M and Pan C-L “Ultrabroadband terahertz field detection by photoconductive antennas based on multi-energy arsenic-ion-implanted GaAs and semi-insulating GaAs.” Appl. Phys. Lett. **Vol.83**, 1322,(2003)
- [21] M. Lambsdorff, J. Kuhl, J. Rosenzweig, A. Axmann, and Jo. Schneider, “Subpicosecond carrier lifetimes in radiation-damaged GaAs.” Appl. Phys. Lett. **Vol.58**, 1881 (1991)
- [22] M. J. Lederer, B. Luther-Davies, H. H. Tan, C. Jagadish, M. Haiml, U. Seifner, and U. Keller, “Nonlinear optical absorption and temporal response of arsenic- and oxygen-implanted GaAs.” Appl. Phys. Lett. **Vol.74**, 1993 (1999)
- [23] B. Salem, D. Morris, V. Aimez, J Veerens, J Beauvais and D Houde.”Pulsed photoconductive antenna terahertz sources made on ion-implanted GaAs substrates” J. Phys.: Condens. Matter 17 7327-7333 (2005)
- [24] M. Mikulics, E. A. Michael, M. Marso, M. Lepsa, A. van der Hart, and H. Lüth, A. Dewald, S. Stanček and M. Mozolik, P. Kordoš, “Traveling-wave photomixers fabrication on high energy nitrogen-ion-implanted GaAs”, Appl. Phys. Lett. **Vol.89**, 071103, (2006)
- [25] B.Salem, D.Morris, Y.Salissou, V.Aimez and S.Charlebois, M.Chicoine, F. Schiettekatte, “Terahertz emission properties of arsenic and oxygen ion-implanted GaAs based photoconductive pulsed sources” J.Vac.Sci. Technol. A 24(3), pp.774-777,(2006)
- [26] B.Salem, D.Morris, V.Aimez, J Beauvais and D Houde, “Improved characteristics of a terahertz set-up built with an emitter and a detector made on proton-bombarded GaAs photoconductive materials” Semicond. Sci. Technol. **Vol.21**, 283-286,(2006)
- [27] P.K. Benicewicz, J.P. Roberts, and A.J. Taylor, “Sacling of terahertz radiation from large-aperture biased photoconductors,” J. Opt. Soc. Am. B, **Vol.11**, pp. 2533-2546, (1994)
- [28] Davi K. Cheng, “Field and Wave Electromagnetics”, 2nd Ed., Addison-Wesley. (1989)

- [29] Justin T. Darrow, Xi Cheng Zhang, David H. Auston, Fellow, IEEE and Jeffrey D. Morse, "Saturation Properties of Large-Aperture Photoconducting Antennas" IEEE Journal of Quantum electronics, **Vol.28**, pp. 1607-1616, (1992)
- [30] Zhisheng Piao, "Carrier Dynamics and Terahertz radiation in Photoconductive Antennas," Jpn. J. Appl. Phys., **Vol.39**, pp.96-100, (2000)
- [31] P. Uhd Jepsn, R. H. Jacobsen, and S. R. Keiding, "Generation and detection of terahertz pulses from biased semiconductor antennas," J. Opt. Soc. Am. B, **Vol.13**, pp. 2424-2436, (1996)
- [32] M. Tani, S. Matsuura, K. Sakai and S. Nakashima, "Emission characteristics of photoconductive antennas based on LT-GaAs and SI GaAs" Appl. Opt., **Vol.36**, No.30, pp. 7853-7859, Oct. (1997)
- [33] S. Verghese, K. A. McIntosh, and E. R. Brown, IEEE Trans. Microwave Theory Tech. 45, 1301 (1997)
- [34] A. W. Jackson, Ph.D. thesis, University of California at Santa Barbara (1999)
- [35] J. C. G. Lesurf. "Millimetre-wave optics, devices and systems." Adam Hilger, January (1990)
- [36] P. K. Benicewicz, J. P. Roberts, and A.J. Taylor, J. Opt. Soc. Am. B 11, 2533 (1994)
- [37] T. Darrow, X.-C. Zhang, and D.H. Auston, "Power scaling of large-aperture photoconducting antennas." Appl. Phys. Lett. **Vol.58**, 25 (1991)